arXiv:1702.02249v1 [hep-ph] 8 Feb 2017

The gluon condensation at high energy hadron collisions

Wei Zhu[a] and **Jiangshan Lan**[b]

[a]Department of Physics, East China Normal University, Shanghai 200241, P.R. China

[b]Institute of Modern Physics, Chinese Academy of Sciences, Lanzhou 730000, P.R. China

Abstract

We report that the saturation/CGC model of gluon distribution is unstable under action of the chaotic solution in a nonlinear QCD evolution equation, and it evolves to the distribution with a sharp peak at the critical momentum. We find that this gluon condensation is caused by a new kind of shadowing-antishadowing effects, and it leads to a series of unexpected effects in high energy hadron collisions including astrophysical events. For example, the extremely intense fluctuations in the transverse-momentum and rapidity distributions of the gluon jets present the gluon-jet bursts; a sudden increase of the proton-proton cross sections may fill the GZK suppression; the blocking QCD evolution will restrict the maximum available energy of the hadron-hadron colliders.

keywords: Gluon condensation; Unstable CGC; Gluon-jet bursts; GZK puzzle; Blocking QCD evolution; Maximum available energy in hadron-hadron collider

PACS numbers: 12.38.-t; 14.70.Dj; 05.45.-a

1 Introduction

The planning of high-energy proton-proton colliders, such as very large hadron collider (VLHC) [1] and the upgrade in a circular e^+e^- collider (SppC) [2] will provide a nice opportunity to discover new phenomena of nature. The hadron collider with the center-of-mass energy of hundred TeV order may probe the parton distribution functions (PDFs) in several currently unexplored kinematical regions. In such ultra low-x region, the PDFs maybe beyond our expectations. Therefore a new exploration of the PDFs in the proton is necessary for any future higher-energy hadron colliders.

The gluon density in nucleon grows with decreasing Bjoeken variable x (or increasing energy $\sqrt{s}$) according to the linear DGLAP Dokshitzer-Gribov-Lipatov-Altarelli-Parisi (DGLAP) [3,4] and Balitsky-Fadin-Kuraev-Lipatov (BFKL) [5] equations, where the correlations among the initial gluons are neglected. At a characteristic saturation momentum $Q_s(x)$, the nonlinear recombination of the gluons becomes important and leads to an eventual saturation of parton densities [6]. This state is specified as the color glass condensate (CGC) [7], where "condensate" implies the maximum occupation number of gluons is $\sim 1/\alpha_s$, although it lacks a characteristic sharp peak in the momentum distribution.

Recently, Zhu, Shen and Ruan proposed a modified BFKL equation in [8,9] (see Eq. (2.1)), where the nonlinear evolution kernels are constructed by the self-interaction of gluons as similar to the Balitsky-Kovchegov (BK) equation [10] and Jalilian-Marian-Iancu-McLerran-Weigert-Leonidov-Kovner (JIMWLK) equation [11], but the former keeps the nonlinear BFKL-singular structure. Using the available saturation models as input, the new evolution equation presents the chaos solution with positive Lyapunov exponents [12], and it predicts a new kind of shadowing caused by chaos, which stops the QCD evolution after a critical small x_c. This unexpected result implies that the predicted saturation state by the BK/JIMWLK dynamics is unstable at the small x range.

In this work, we study continually the properties of this new evolution equation. We report that chaos in this equation converges gluons to a state at a critical momentum. This distribution with a stable sharp peak indicates that it is the gluon condensation (see Figs. 1 and 2). We present the evolution process from a saturated input to the gluon condensed state in Sec. 2. We find that the chaotic oscillations of the gluon density raise both the strong negative and positive nonlinear corrections. The former shadows the grownup of the gluon density, while the later is the antishadowing effect. The antishadowing as a positive feedback process increases rapidly the gluon density. Thus, we observed the gluon condensation at the critical momentum (x_c, k_c).

The sharp peak in the gluon distribution is higher than the normal distribution by several orders of magnitude due to a lot of gluons accumulated in a narrow momentum space. The gluon condensation should appear significant effects in the hadron processes (see Sec. 3), provided the position of x_c inters the observable range at high energy. Obviously, we have not yet found any signals of the above mentioned gluon condensation even at the proton-proton collider with $E_{CM} = 14\ TeV$ in LHC. Therefore, we turn to the ultra high energy cosmic rays (UHECRs) in Sec. 4, where the proton energy is much larger then that in the accelerators. We find that a sudden increase of the proton-proton cross section may fill the Greisen-Zatsepin-Kuzmin (GZK) suppression [13]. Using this result we estimate the value of x_c.

Based on the results of Sec. 4, we predict the possible experimental observations of the gluon condensation in the future high-energy proton-proton colliders in Sec. 5. We find that the gluon condensation may bring the big fluctuations of the gluon jets at the high-energy proton-proton collider. The gluons in every sub-jet are monochromatic and coherent, we call them as the gluon-jet bursts. Such intensive gluon field provides an ideal laboratory to study QCD at the extreme conditions. We should pay attention to the

big effects of the gluon-jet bursts when planning the next high energy hadron colliders and the detectors. We also predict a maximum available energy of the hadron colliders due to the blocking QCD evolution. Finally, we discuss the reasonableness of the gluon condensation in Eq. (2.1) from some general considerations in Sec. 6. A summary is given in Sec. 7.

2 The gluon condensation caused by chaos

A modified BFKL equation for the unintegrated gluon distribution $F(x,k_T^2)$ at the leading logarithmic ($LL(1/x)$) approximation is [9]

$$
\begin{aligned}
&-x\frac{\partial F(x,k_T^2)}{\partial x} \\
&=\frac{3\alpha_s \underline{k}^2}{\pi}\int_{\underline{k}_0^2}^{\infty}\frac{dk_T'^2}{k_T'^2}\left\{\frac{F(x,k_T'^2)-F(x,k_T^2)}{|k_T'^2-k_T^2|}+\frac{F(x,k_T^2)}{\sqrt{k_T^4+4k_T'^4}}\right\} \\
&-\frac{81}{16}\frac{\alpha_s^2}{\pi R_N^2}\int_{k_0^2}^{\infty}\frac{dk_T'^2}{k_T'^2}\left\{\frac{k_T^2F^2(x,k_T'^2)-k_T'^2F^2(x,k_T^2)}{k_T'^2|k_T'^2-k_T^2|}+\frac{F^2(x,k_T^2)}{\sqrt{k_T^4+4k_T'^4}}\right\},
\end{aligned}
\tag{2.1}
$$

where we used $F(x/2,k_T^2)\simeq F(x,k_T^2)$ near the saturation scale; the value of $R_N=4GeV^{-1}$ is fixed by fitting the available experimental data about the proton structure function. The singular structure both in the linear and nonlinear evolution kernels corresponds to the random evolution in the k_T-space, where $k_T^2-k_T'^2$ may across over zero. This is a general requirement of the logarithmic $(1/x)$ resummation.

In this section we study the properties of Eq. (2.1) using the Golec-Biernat and Wusthoff (GBW) saturation model [14] as the input at x_0

$$
\mathcal{F}_{GBW}(x,k_T^2)=\frac{3\sigma_0}{4\pi^2\overline{\alpha}_s}R_0^2(x)k_T^2\exp(-R_0^2(x)k_T^2), \tag{2.2}
$$

where $\sigma_0=29.12\ mb$, $x_0=4\times10^{-5}$, $\lambda=0.277$, $R_0(x)=(x/x_0)^{\lambda/2}/Q_s$ and $Q_s=1\ GeV$; $\mathcal{F}\equiv F/k_T^2$ and the parameter $\overline{\alpha}_s$ is fixed as $\overline{\alpha}_s=0.2$. Note that in the calculation we take $F(x,k_T^2)=0$ if $F(x,k_T^2)<0$ since $F(x,k_T^2)\geq 0$ according to the definition of the gluon distribution.

The chaotic solutions of Eq. (2.1) exist around $k_c\sim Q_s\sim 1\ GeV$, where perturbative calculations are barely available. However, more lower k_T-range should be included, for example, we take $k_0=0.1\ GeV$. The region at $k_T^2<1\ GeV^2$ is a complicate range, where coexisting perturbative and non-perturbative effects. For avoiding the difficulty in the

infrared region, the evolution region was divided into two parts at $Q_s = 1\ GeV$ in the previous work [9]. This is not a smooth treatment and it may deform the effects of the chaotic solutions.

Fortunately, many works have discussed the low Q^2 transition region from the perturbative side [15]. They incorporate in an effective non-perturbative corrections into the evolution calculations. Considering the non-perturbative dynamics of QCD generate an effective gluon mass at very low Q^2 region, and its existence is strongly supported by QCD lattice simulations [16]. This dynamical gluon mass is intrinsically related to an infrared finite strong coupling constant. According to this idea, the suppressed strong coupling constant can be used at low Q^2 and we take a following restriction

$$\alpha_s \leq \alpha_{s,Max} \equiv B, \tag{2.3}$$

the constant B describes the non-perturbative corrections and we take $B = 0.5$ as an example. We will indicate that our results are insensitive to the value of B in a reasonable range. Thus, we can expand our perturbative calculation to $k_0 = 0.1\ GeV$.

The x-dependence of $F(x, k_T^2)$ with different values k_T^2 are illustrated in Fig. 1. It is surprise that one (thick) line with $k_c^2 = 0.654\ GeV^2$ approaches to a large positive value at $x \to x_c = 6 \times 10^{-6}$, (this line has not been reported in Ref. [9]); while all other lines with $k_T^2 \neq k_c^2$ drop suddenly to zero. This result seems that the gluons in the proton converge to a state with a critical momentum (x_c, k_c).

The k_T^2-dependence of $F(x, k_T^2)$ in Fig. 2 more clearly shows the evolution of the gluon distribution from the saturated input to the condensed state step by step. This result indicates that a lot of gluons in the proton converge to a state at a critical momentum (x_c, k_c), i.e. a typical gluon condensation.

Figure 3 presents the value x_c with different parameter $\alpha_{s,Max}$ in Eq. (2.3). We find

that the gluon condensation still exists in a reasonable range of $\alpha_{s,Max}$.

We recalculated Eq. (2.1) but the evolution region was divided into perturbative and non-perturbative region and treated separately as in Ref. 9. In this method, the evolution region has two parts: region(A) 0 to Q_s^2 and region(B) Q_s^2 to ∞. In region(B) the QCD evolution equation (2.1) is taken to evolute and in region(A) the nonperturbative part of $F(x, k^2)$ is identified as

$$F(x, \underline{k}^2) = C\underline{k}^2 \mathcal{F}_{GBW}(x, \underline{k}^2), \quad at\ x \leq x_0,\ \underline{k}^2 \leq Q_s^2, \tag{2.4}$$

where the parameter C keeps the connection between two parts. The results are shown in Figs. 4 and 5, where the dashed lines are proportional to the GBW input according to Eq. (2.4). We find the peak at x_c similar to Fig. 1, but the k_T-dependent structure of $F(x, k_T^2)$ near x_c is completely distorted due to Eq.(2.4), which shadows the evolution of the condensation at $k_T^2 < k_c^2$. Note that if we removed the dashed lines from Figs. 4 and 5, the results are consistent with Figs. 1 and 2. Therefore, the treatment in Eq. (2.4) hiders our understanding of the condensation solution.

One can understand the above gluon condensation as follows. As work [9] has pointed out that the derivative structure $\sim \partial F(x, k_T^2)/\partial k_T^2$ and $\sim \partial F^2(x, k_T^2)/\partial k_T^2$ in Eq. (2.1) add a perturbation on the smooth curve $F(x, k_T^2)$ once k_T crosses over Q_s. Thus, we have a series of independent perturbations in a narrow k_T domain near Q_s along evolution to smaller x. In the linear BFKL equation, these perturbations are independent and their effects are negligibly small. In this case the solutions keep the smooth curves in (x, k_T^2) space. However, the nonlinear Eq. (2.1) may form chaos near Q_s. The positive Lyapunov exponents of Eq. (2.1) in Fig. 6 support this suggestion. Note that once chaos is produced, the fast oscillations of the gluon density produce both the negative and positive nonlinear corrections to $\Delta F(x, k_T^2)$ through the derivative structure of Eq. (2.1). The former

shadows the grownup of the gluon density, while the later is the antishadowing effect, and it increases festally the gluon density because it is a strong positive feedback process. A maximum distribution $F(x \sim x_c, k_T^2 \sim k_c^2)$ in Fig. 1 will result a pair of closer and more stronger positive and negative corrections at a next evolution step, where the positive correction continually put $F(x, k_T^2)$ toward to a biggest value, while the negative one suppress all remain distributions. Thus, we observed the gluons condensation at (x_c, k_c^2) due the extrusion of the shadowing and antishadowing effects in the QCD evolution. Comparing with the CGC, Figs. 1 and 2 show a really gluon condensation in the gluon distribution.

The peak value $F(x_c, k_c^2)$ is uncertain, although it is a big value. According to the character of the condensate, the infinite Bosons converge to a same point on the phase space, an ideal $F(x, k_T^2)$ at (x_c, k_c^2) is the delta-function. However, any measurable distribution $F(x_c, k_c^2)$ has a width and the corresponding peak value is finite, which depends sensitively on the measurement conditions and even on the calculating precision. Therefore, the precise value of $F(x_c, k_c^2)$ should be determined by the experiments.

3 The effects of the gluon condensation

The gluon condensation in the example of Sec. 2 produces the big corrections to the normal parton distributions even by several orders of magnitude. Such strong signals should appear in the experimental data if the probe enters an enough lower x range containing x_c.

Unfortunately, we can not determine the value of x_c in the theory since several uncertainties. For example, the value of x_c relates sensitively to the starting position x_0 of Eq. (2.1), which is really unknown although we assumed $x_0 = 4 \times 10^{-5}$ at Sec. 2. A similar example is the BFKL equation. Usually we assume that the BFKL equation starts work at $x \sim 10^{-3} - 10^{-4}$, however, the most PDF databases apply the DGLAP equation till to $x << 10^{-3}$. Besides, the uncertainties of the parameters in Eqs. (2.1) and (2.2) also hider us to predict the value of x_c. Therefore, we take the following program to make the estimations of the gluon condensation effects: In this section we take the example of Sec. 2 to study the effects of the gluon condensation, then we transplant the results to astrophysics, where we may obtain the information about the value of x_c. Finally, we predict the signals of the gluon condensation in the future hadron colliders using the determined x_c.

The cross section of inclusive particle production in high energy proton-proton collision is dominated by the production of gluon mini-jet using the unintegrated gluon distribution via [17,18]

$$\frac{d\sigma}{dk_T^2 dy} = \frac{64N_c}{(N_c^2-1)k_T^2}\int_{0.1}^{100} q_T dq_T \int_0^{2\pi} d\phi \alpha_s(\Omega) \frac{F(x_1, \frac{1}{4}(k_T+q_T)^2)F(x_2, \frac{1}{4}(k_T-q_T)^2)}{(k_T+q_T)^2(k_T-q_T)^2}, \tag{3.1}$$

where $\Omega = Max\{k_T^2, (k_T+q_T)^2/4, (k_T-q_T)^2/4\}$; The longitudinal momentum fractions of interacting gluons are fixed by kinematics: $x_{1,2} = k_T e^{\pm y}/\sqrt{s}$; The distribution $F(x, k_T^2)$

is taken from the results in Sec. 2 but they are multiplied by $(1-x)^4$ for expanding to $x > x_0$.

The rapidity distribution of the gluon-jets

$$\frac{d\sigma}{dy} = \int_{x_c^2 s e^{\mp 2y}}^{100} dk_T^2 \frac{d\sigma}{dk_T^2 dy}, \tag{3.2}$$

where if $x_c^2 s e^{\mp 2y} < 0.3\ GeV^2$ we fixed it as $0.3\ GeV^2$. The part of results at different $\sqrt{s}$ are presented (solid lines) in Fig. 7. We find that the large fluctuations arisen by the gluon condensation. The gluon condensation effects begin work from $\sqrt{s_{GC}} \simeq 200\ GeV$ in this example. The relation between x_c and $\sqrt{s_{GC}}$ is kinematically determined as follows. Note that the gluon condensation plays a role if the contributions of the gluon condensation peak local at $y_{Max} = \ln(\sqrt{s}/k_{T,Min})$, i.e.,

$$x_c = \frac{k_T}{\sqrt{s_{GC}}} e^{-y_{Max}} = \frac{k_T k_{T,Min}}{s_{GC}} \simeq \frac{k_{T,Min}^2}{s_{GC}}. \tag{3.3}$$

In the example Fig. 7, the resulting $\sqrt{s_{GC}} \simeq 200\ GeV$.

For the comparison, we plot the solutions removed the gluon condensation by broken lines in Fig. 7, (i.e., the peak-like distribution is removed from $F(x, k_T^2)$). The dashed lines are the solutions using the GBW input but without the QCD evolution. Comparing these lines, one can find the strong effects caused by the gluon condensation in hadron collisions. Unfortunately, we never got any repots about these effects till at the proton-proton collider with $E_{CM} = 14\ TeV$ in LHC. Therefore, we suggest that $x_c << 6 \times 10^{-6}$. In next section we try to determine the value of x_c using the possible signals of the gluon condensation in astrophysics, where the energy scale of the proton-proton interaction may be more larger then that in the accelerators.

4 The gluon condensation and the GZK puzzle

Before 50 years, Greisen, Zatsepin and Kuz'min [13] predicted a drastic reduction of the spectrum of cosmic rays around the energy of $E = (2 \sim 5) \times 10^{19}\ eV$, since energy losses of the cosmic rays in the cosmic microwave background radiation during their long propagation. This is the GZK cutoff.

The mean free path for photoproduction is calculated by $\lambda_{\gamma p} = 1/(N\sigma)$, where N is the number density of blackbody photons and $\sigma(\gamma p \to \pi^0 p) \simeq 100\mu b$ is the cross section at threshold. This leads to $\lambda_{\gamma p} \simeq 10Mpc$. The Markarian galaxies are the nearest possible UHECR-sources, which are residing at distances of approximately $x \sim 100Mpc$. The arrival probability of protons through these distances with energies exceeding $10^{20}eV$ is only $\sim e^{-x/\lambda_{\gamma p}} = 10^{-4} - 10^{-5}$. However, the observations defy this result [19-21], where the recent Auger data seem to diminish by steps only in one order of magnitude, but not by an abrupt descend as above conceived. A big gap presents between theory and experiments. Many ideas and different models are proposed to understand the GZK puzzle even suspecting the Lorentz invariance and the Standard Model, however, the true answer of the GZK puzzle is still far from knowing.

We noticed the following facts: since the flux of UHECRs is so low, direct measurement of properties of UHECRs on the earth is impractical. One must measurement is the extensive air shower on the earth, which is created when cosmic ray enters the atmosphere.

The total cross section measured in the proton-proton collision is generally defined as

$$\sigma = \frac{J}{n_{beam}}, \tag{4.1}$$

where J is the total number of measured interactions and $n_{beam} = J_0/\sigma_0$ is the number of beam particles per unit σ_0 of transverse area. Therefore, the detected UHECR flux on the earth reads

$$J(E) = \frac{\sigma(\sqrt{s})}{\sigma_0} J_0(E), \tag{4.2}$$

where $J_0(E)$ is the primary flux of UHECRs; σ is the interaction cross section of the proton in the UHECRs with the atmospheric proton. Note that the GZK energy scale $E \sim 2 \times 10^{19}\ eV$ corresponds to the total energy in the center of mass (CM) frame $\sqrt{s} \sim 200\ TeV$ using $\sqrt{s} \simeq \sqrt{2m_N E}$; E is the interaction energy in the rest frame of the target proton. Obviously, such energy far exceed the energy of existing particle accelerators. There are no any reasons to indicate that the cross section σ at $\sqrt{s} > 200\ TeV$ still keeps the traditional estimation. We assume that the value of x_c is enough small, and a sudden increase of the proton-proton cross section at such GZK-scale due to he gluon condensation may fill the GZK suppression.

Now let us to realize this idea. At first step, we calculate the corrections of the gluon condensation to the cross section of proton-proton collision in the example of Secs. 2-3, where $x_c = 6 \times 10^{-6}$ is used. We define the rate

$$R(\sqrt{s}) \equiv \frac{\int dy \frac{d\sigma(\sqrt{s})}{dy}}{\int dy \frac{d\sigma_{naive}(\sqrt{s})}{dy}}, \tag{4.3}$$

where σ_{naive} is the cross section without the QCD evolution (dashed lines in Fig. 7). The rate R represents the corrections of the gluon condensation to the proton-proton cross section at different scale $\sqrt{s}$. The results are shown in Fig. 8a.

In the next step, we transplant the results with $x_c = 6 \times 10^{-6}$ to a more small critical value $x_c^I \ll x_c$. For this sake, we need a new set of $F(x, k_T^2)$ with $x_0 \ll 4 \times 10^{-5}$. For simplicity, we take an indirect way to do them. We have pointed out that the strong gluon condensation effects are dominated by the peak distribution $F(x_c, k_c^2)$ at x_c. According to Eq. (3.3) we use

$$\frac{x_c}{x_c^I} = \frac{s_{GC}^I}{s_{GC}} \to \frac{s^I}{s} \tag{4.4}$$

to estimate the value of x_c^I corresponding to s_{GC}^I. The above last step assumes that this scale transform is valid at $s > s_{GC}$. Thus, if the gluon condensation begins work at the GZK scale $E = 2 \times 10^{-19}\ eV$ (or $\sqrt{s_{GC}^I} = 200\ TeV$), we should choose $x_c^I = 6 \times 10^{-12}$. Using this result and Fig. 8a we modify the proton-proton cross section at $\sqrt{s^I} \geq 200\, TeV$ as $\sigma(s) \to \sigma^I(s^I) = \sigma(s^I)/R(s^I)$ in Eq. (4.2), where a new s^I scale in Fig. 8a is used. Figure 9 shows the cosmic-ray energy spectrum measured by the Auger collaboration [21]. The spectrum is divided by $E^{-2.67}$. The open point and open star are the results of the Auger data divided by R in Fig. 8a. The solid line in Fig. 9 is a smoothing result. It is surprise that the gluon condensation may suddenly enhance the proton-proton cross section by almost four orders of magnitude, they may fill the GZK suppression.

The index in the power law $J \propto E^{-\gamma}$ in our results is $\gamma \simeq 17$ at $2 \times 10^{19} - 3 \times 10^{19}\ eV$. It is much larger than the power index $\gamma = 2.67$ at $E < 2 \times 10^{-19}\ eV$ and presents a sudden fall in the energy spectrum as predicted by GZK cutoff.

We consider another possible choice of x_c: the gluon condensation starts from $\sqrt{s_{GC}^{II}} = 80\, TeV$, where is a position of the ankle at $E = 3.5 \times 10^{18}\ eV$. In this case, $x_c^{II} = 4 \times 10^{-11}$. The results using Fig. 8b are presented by the dashed line in Fig. 9.

The flux $J_0(E)$ can be estimated by the interaction length $L(E)$ using [22]

$$J_0(E) \simeq \frac{1}{4\pi} L(E) \Phi(E), \tag{4.5}$$

where the local injection spectrum $\Phi(E)$ has a power-law form of the hadron spectrum $\sim E^{-2.67}$ in energy. We can not determine $J_0(E)$ since the position of the UHECR-source is not fixed. However, the generally expected proton interaction length quickly reduces a few orders of magnitude at the GZK scale [22,23], and this is consistent with our results in Fig. 9.

The saturation and condensation origin from the BK and Eq. (2.1), respectively.

One can understand a big difference between the starting points of these two evolution equations. The nonlinear terms in the BK equation exclude the contributions of the gluon recombination in the cross-channels [24]. These processes are considered by Eq. (2.1) at more higher density of gluons, where the correlations among gluons becomes stronger. However, the enhancement of the gluon density with increasing x at the saturation range is very slow due to a big shadowing. Therefore, the starting point x_0 of the evolution in Eq. (2.1) is much smaller than that in the BK equation.

We noted that the Auger collaboration reported [25] that the proton-proton cross section at $\sqrt{s} = 57\ TeV$ is a normal value $\sim 505\ mb$. This energy scale is close to $\sqrt{s^{II}_{GC}} = 80\ TeV$. However, the result is derived indirectly from the distribution of the depths of shower maximum, its tail is sensitive to the cross section. We think that the true shower shape originates from the condensate gluons, therefore, it is different from the normal shower shape since the coherence among the gluons at x_c. Therefore, we can not exclude a strong proton-proton cross section at this energy scale.

5 The gluon condensation at the future hadron colliders

The projected high energy proton-proton collisions will probe deeply the very low x domain, where we may observe the gluon condensation. According to the GZK cutoff we have two possible choices: (i) $\sqrt{s^I_{GC}} = 200\ TeV$, $x^I_c = 6 \times 10^{-12}$; (ii) $\sqrt{s^{II}_{GC}} = 80\ TeV$, $x^{II}_c = 4 \times 10^{-11}$. We give the rapidity distributions of the gluon jets at proton-proton collision with $E_{MC} = 100\ TeV$ in Figs. 10a and 10b for these two assumptions, where y-scale is re-plotted using $y_{Max} = \ln(\sqrt{s^{I(II)}}/k_{Min})$. We find that in the x^{II}_c case, the gluon condensation effect is obvious.

The fluctuation structure also appears in the transverse-momentum distributions of the gluon jets

$$\frac{d\sigma}{dk_T} = 2k_T \int_0^{y_{Max}} dy \frac{d\sigma}{dk_T^2 dy}. \tag{5.1}$$

The results are shown in Fig. 11, where the broken and dashed lines are the results from removing the contributions of the gluon condensation and the input distribution without QCD evolution, respectively. The results show that the contributions of the gluon condensation are constructed by many sub-jets. The strength of these sub-jets is much higher then the normal distribution. The gluons inside every sub-jet are dominated by the condensate gluons, they have same energy-momentum. In particulary, these gluons are created at a same collision time and have the same phase. Therefore, the gluons in every sub-jet are monochromatic and coherent. We call the phenomena in Figs. 10 and 11 as the gluon-jet bursts. Although our estimations are rough, such extremely intense gluon field are the ideal laboratory studying QCD at the extreme conditions. We should pay attention to the big effects of the gluon-jet bursts when planning the next high energy hadron colliders and the detectors.

The nuclear target may increase the value of x_c since the nonlinear corrections need to be multiplied by $0.5A^{1/3}$ in a nucleus-nucleus collider [26], where the factor 0.5 is from the nuclear geometric corrections. We take $Pb-Pb$ collider as the example, the numeric solutions of Eq. (2.1) show that

$$\frac{x_c}{x_{c;Pb-Pb}} \simeq \frac{x_c^{I(II)}}{x_{c;Pb-Pb}^{I(II)}}. \tag{5.2}$$

We get $x_{c;Pb-Pb}^{I} = 2 \times 10^{-11}$ and $x_{c;Pb-Pb}^{II} = 10^{-10}$. Using Eq. (4.4) we present our predictions in Figs. 12-15.

E. Fermi predicted jokingly that a maximum accelerator will around the equator. However, there is an applicable maximum energy for the hadron-hadron collider. At high energy (or at small x), the total cross section of the collision is responsible for the gluon distributions in the beam nucleons. The gluon condensation implies that the gluons with $x < x_c$ converge to a critic state at $x = x_c$, which leads to $F(x < x_c, k_T^2) = 0$. This prediction should be presented in the measurable cross section σ_{p-p}. Note that for a given collision energy, only the partons in a certain kinematic range are effectively used due to the kinematic restriction. We image that the condensate peak begins work at $\sqrt{s_{GC}}$. As we have shown in Figs. 7 and 8, it rises a sudden big increase of the proton-proton cross sections, and this effect expands till $\sqrt{s_{Max}}$. On the other hand, $F(x < x_c, k_T^2)$ will dominate the parton interacting range if $\sqrt{s} > \sqrt{s_{Max}}$. The results in Fig. 7 show that the gluon contributions to the hadron collider almost disappear when the position of the condensation peak approaches to the rapidity center $y = 0$. The last three diagrams in Fig. 7 present this situation, where the missing part of the rapidity distribution corresponds to the disappearance of gluons at $x < x_c$ in Fig. 1. One can estimate the corresponding energy scale $\sqrt{s_{Max}}$ using Figs. 7 and 8. We find that $\sqrt{s_{Max}^{I}} \simeq 10^6\ TeV$, or $\sqrt{s_{Max}^{II}} \simeq 10^5\ TeV$ for our two assumptions. Beyond this energy

scale, σ_{pp} is almost small, where the remaining small contributions are from the quarks and Abelian gluons [9]. It implies that a proton beam becomes "transparent", therefor, the high energy collider is inefficient at $\sqrt{s} > \sqrt{s_{Max}}$. We call $\sqrt{s_{Max}}$ as the maximum applicable energy of the proton-proton collider.

A purpose of the high energy collider is to convert the kinetic energy of the beam nucleons into the creating new particles. A big cross section σ_{p-p} implies a high rate of this conversion. Therefore, $\sqrt{s} = 100 - 10^6\ TeV$ is a golden energy range for the proton-proton collider.

6 Discussions

The equation (2.1) is based on the leading QCD approximation, where the higher order corrections are neglected. An important question is: will disappear the chaos effects in the evolution equation after considering higher order corrections? We answer this question from two different aspects.

(i) As we have pointed out that chaos in the modified BFKL equation origins from the special singularity of the nonlinear evolution kernel. From the experiences in the study of the BFKL equation, the higher order QCD corrections can not remove this primary singularity [27]. Let us assume that Eq.(2.1) is modified as following form if considering the higher order corrections

$$
\begin{aligned}
&-x\frac{\partial F(x,k_T^2)}{\partial x} \\
&= \frac{3\alpha_s k_T^2}{\pi}\int_{k_0^2}^{\infty}\frac{dk_T'^2}{k_T'^2}\left\{\left[\frac{F(x,k_T'^2)-F(x,k_T^2)}{|k_T'^2-k_T^2|}+\frac{F(x,k_T^2)}{\sqrt{k_T^4+4k_T'^4}}\right]\left[\left[1+A(k_T'^2,k_T^2)\right]\right\}\right. \\
&\left.-\frac{81}{16}\frac{\alpha_s^2}{\pi R_N^2}\int_{k_0^2}^{\infty}\frac{dk_T'^2}{k_T'^2}\left\{\left[\frac{k_T^2F^2(x,k_T'^2)-k_T'^2F^2(x,k_T^2)}{k_T'^2|k_T'^2-k_T^2|}+\frac{F^2(x,k_T^2)}{\sqrt{k_T^4+4k_T'^4}}\right]\left[1+B(k_T'^2,k_T^2)\right]\right\}\right.. \qquad (6.1)
\end{aligned}
$$

One can image that the contributions from $A(k_T'^2,k_T^2)$ and $B(k_T'^2,k_T^2)$ either are the smooth function of $k_T'^2$ and k_T^2, or have the extra singular structure. In the former case, we take an approximation: A and B are almost constant and

$$
\begin{aligned}
&-x\frac{\partial F(x,k_T^2)}{\partial x} \\
&= \frac{3\alpha_s k_T^2}{\pi}\int_{k_0^2}^{\infty}\frac{dk_T'^2}{k_T'^2}\left\{\left[\frac{F(x,k_T'^2)-F(x,k_T^2)}{|k_T'^2-k_T^2|}+\frac{F(x,k_T^2)}{\sqrt{k_T^4+4k_T'^4}}\right]\beta\right\} \\
&-\frac{81}{16}\frac{\alpha_s^2}{\pi R_N^2}\int_{k_0^2}^{\infty}\frac{dk_T'^2}{k_T'^2}\left\{\left[\frac{k_T^2F^2(x,k_T'^2)-k_T'^2F^2(x,k_T^2)}{k_T'^2|k_T'^2-k_T^2|}+\frac{F^2(x,k_T^2)}{\sqrt{k_T^4+4k_T'^4}}\right][1-\beta]\right\}. \qquad (6.2)
\end{aligned}
$$

We give the predicted value x_c with different values of β in Fig. 16. One can find that the gluon condensation solution is insensitive to the parameter β in its reasonable range.

In the second case, Eq. (2.1) may have the multi-chaos solution. For example, we take the Fadin-Lipatov (KL) model [28] as the input to study Eq. (2.1), i.e.,

$$F(x_0, k_T^2) = \begin{cases} f_0 k_T^2 \ if \ k_T^2 < Q_s^2 \\ f_0 Q_s^2 \ if \ k_T^2 > Q_s^2 \end{cases} \tag{6.3}$$

The solution shows two positive peaks in Fig. 17, which correspond to two maximum values of Lyapunov exponents in Fig. 18. One of them arris from a non-smooth connection at $k_T^2 = Q_s^2$ in Eq. (6.3). However Fig. 19 shows that these two chaos lead to the gluon condensation at a critic value x_c because the competition among several positive feedback processes. This conclusion has a general mean: if existing the multi-singular structure from the higher order corrections, the corresponding nonlinear evolution equation still has the gluon condensation.

(ii) We discuss the approximation solution of Eq. (2.1) from the view point of the chaos theory. It is well known that some of chaotic attractors are unstable. A slight fluctuation of a parameter may drive the system out of chaos. However, it has been proofed that some dynamical systems can exhibit robust chaos [29]. A chaotic attractor is said to be robust if, for its parameter values, there exist a neighborhood in the parameter space with absence of periodic negative Lyapunov exponents. Robustness implies that the chaotic behavior cannot be destroyed by arbitrarily small perturbations of the system parameters. The structure of the Lyapunov exponents in Figs. 6 and 18 show absence of any negative values around $k_T^2 \sim 1 \ GeV^2$, and the maximum value of λ is enough larger $\lambda \gg 1$. This means that chaos in Eq. (2.1) is robust. Therefore, we expect that chaos and its effects still exist even considering the higher order corrections.

The above analysis tell us that the gluon condensed effects origin from the singular

nonlinear evolution kernel, which is a general structure in the logarithmic $(1/x)$ resummation. Now we point out that the gluon condensation is a nature result of the momentum conservation. We call the positive corrections of the nonlinear terms in a QCD evolution equation as the antishadowing, which is the compensation to the shadowing effect due to the momentum conservation [30]. There are two different antishadowing effects: one was presented in a modified DGLAP equation [31] and a modified BK equation [24], where the antishadowing effect compensates the lost momentum in shadowing. Since in these examples the shadowing is smaller and the increasing gluons distribute in a definite kinematic range, such antishadowing effect is weaker and it consists with the observed EMC effects [32]. On the other hand, in the gluon condensation, a lot of gluons compensate the disappearing gluons at $x < x_c$, and they accumulate at a same critic momentum. In consequence, a sharp peak is added on the gluon momentum distribution and it creates a series of strong effects. Therefore, the gluon condensation is an inevitable result due to the momentum conservation for compensating the lost momenta in the blocking QCD evolution.

7 Summary

A QCD evolution equation at small x should sum the contributions of the gluon random evolution on the transverse-momentum space. The evolution kernels of this equation have singular structure even in the nonlinear kernels. A standard regularization technic is to sum the contributions of the virtual diagrams according to the unitary theory. The resulting evolution kernels have approximately the derivation form with k_T. A modified nonlinear BFKL equation Eq. (2.1) is a such example.

Equation (2.1) has the robust chaotic solution arising from its nonlinear singular structure if the input distribution has an obvious deformation likes the saturation form around $k_T \sim Q_s$.

In this work we present that the dramatic chaotic oscillations produce the strong shadowing and antishadowing effects, they converge gluons at $x < x_c$ to a state with a critical momentum (x_c, k_c). This is the gluon condensation and the blocking QCD evolution.

The sharp peak in the momentum distributions caused by the gluon condensation implies a large enhancement of the cross section in hadron-hadron collision. We examine that the sudden increase of the proton-proton cross section by several orders of magnitude may fill the GZK suppression. Using this result we extract the critic parameter x_c. Then we predict the possible observations of the gluon condensation effects in the future hadron colliders. We predict a maximum applicable energy of the hadron collider due the blocking QCD evolution of the gluons. We find that the gluon condensation leads to the big fluctuations of the gluon jets in its rapidity and transverse-momentum distributions at a ultra high energy range. The gluons in every sub-jet are monochromatic and coherent, and we call them as the gluon-jet bursts. Such extremely intense gluon field caused by the gluon condensation is an ideal laboratory to study QCD at the extreme-conditions.

We should pay attention to the big effects of the gluon-jet bursts when planning the next high energy hadron colliders and the detectors.

Acknowledgments: We thank F. Wang for useful discussions. We would also like to thank X.R. Chen for organizing a meeting in IMP, where we discussed the gluon condensation. One of us (J.S.L) thanks H.K. Dai, J.H. Ruan and R. Wang for their help.

References

[1] The Very Large Hadron Collider (VLHC), http://www.vlhc.org.

[2] CepC-SppC Preliminary Conceptual Design Report Vol. II Accelerator, IHEP - CEPC-DR-2015-01, IHEP-AC-2015-01 (2015).

[3] V.N. Gribov and L.N. Lipatov, Sov. J. Nucl. Phys. **15** (1972); Yu.L. Dokshitzer, Sov. Phys. JETP. **46** (1977) 641;

[4] G. Altarelli and G. Parisi, Nucl. Phys. **B126** (1977) 298.

[5] L. N, Lipatov, Sov. J. Nucl. Phys. **23** (1976) 338; V. S. Fadin, E.A. Kuraev and L. N. Lipatov, Phys. Lett., **B60** (1975) 50; E. A. Kuraev, L.N. Lipatov and V. S. Fadin, Sov. Phys. JETP. **44** (1976) 443; E. A. Kuraev, L.N. Lipatov and V. S. Fadin, Sov. Phys. JETP. **45** (1977) 199; I.I. Balitsky and L.N. Lipatov, Sov. J. Nucl. Phys. **28** (1978) 822.

[6] L.D. McLerran, R. Venugopalan, Phys. Rev. **D49** (1994) 2233; ibid. **49** (1994) 3352; ibid. **50** (1994) 2225.

[7] E. Iancu, R. Venugopalan, Quark Gluon Plasma 3, Eds. R.C. Hwa, X.N. Wang, World Scientific, hep-ph/0303204; H.Weigert, Prog. Part. Nucl. Phys. **55** (2005) 461; F. Gelis, E. Iancu, J. Jalilian-Marian, R. Venugopalan, arXiv:1002.0333.

[8] W. Zhu, Z.Q. Shen and J.H. Ruan, Chin. Phys. Lett. **25** (2008) 3605.

[9] W. Zhu, Z.Q. Shen and J.H. Ruan, Nucl. Phys. **B911** (2016) 1.

[10] I. Balitsky, Nucl. Phys., **B463** (1996) 99; Yu. Kovchegov, Phys. Rev. **D60** (1999) 034008; Yu. Kovchegov, Phys. Rev., **D61** (2000) 074018.

[11] J. Jalilian-Marian, A. Kovner, L. McLerran, and H. Weigert, Phys. Rev. **D55** (1977) 5414; J. Jalilian-Marian, A. Kovner, A. Leonidov, and H. Weigert, Nucl. Phys. **B504** (1977) 415; H. Weigert, Nucl. Phys. **A703** (2002) 823.

[12] Ott, E. Chaos in Dynamical Systems, Cambridge University Press, Cambridge, 1993 ; K.T. Alligood, T.D. Sauer, J.A. Jork, Chaos: An Introduction to Dynamical Systems, Springer-Verlag, New York, 1996.

[13] K. Greisen, Phys. Rev. Lett. **16** (1966) 748; G. T. Zatsepin and V. A. Kuzmin, JETP. Lett. **4** (1966) 78.

[14] K. Golec-Biernat and M. Wüsthoff, Phys. Rev. **D59** (1998) 014017; ibid. **D60** (1999) 114023.

[15] C. Aguilar, D. Binosi, J. Papavassiliou and J. Rodriguez-Quintero, Phys. Rev. **D80** (2009) 085018; S.J. Brodsky, G.F. de Teramond and A. Deur. Phys. Rev. **D81** (2010) 096010; E.G.S. Luna, A.A. Natale and A.L. dos Santos Phys. Lett. **B698** (2011) 52.

[16] F.D.R. Bonnet, et al., Phys. Rev. **D64** (2001) 034501; P.O. Bowman, et al., Phys. Rev. **D70** (2004) 034509; Ph. Boucaud, et al., JHEP **0606** (2006) 001; D. Dudal, O. Oliveira, N. Vandersickel Phys. Rev. **D81** (2010) 074505.

[17] L. V. Gribov, E. M. Levin, and M. G. Ryskin, Phys. Rep. **100** (1983) 1.

[18] A. Szczurek, Acta Phys. Pol. **B34** (2003) 3191.

[19] J. Linsley, Phys. Rev. Lett. **10** (1963) 146; World Data Center for Cosmic Rays, Catalogue for Highest Energy Cosmic Rays, No. 2, Institute of Physical and Chemical Research, Itabashi, Tokyo (1986); Efimov, N.N. et al., Astrophysical Aspects of the Most Energetic Cosmic Rays, M. Nagano and F. Takahara, Eds., (World Scientific, Singapore, 1991) p. 20.

[20] R. Abbasi et al. [HiRes Collaboration], Phys. Rev. Lett. **100** (2008) 101101 [arXiv:astroph/ 0703099].

[21] J. Abraham et al. [The Pierre Auger Collaboration], The Cosmic Ray Energy Spectrum and Related Measurements with the Pierre Auger Observatory, arXiv:0906.2189

[22] P. Bhattacharjee and G. Sigl, Phy. Rept. **327** (2000) 109.

[23] D. De. Marco, P. Blasi, A. V. Olinto. Astropart.Phys. **20** (2003) 53; M. De. Domenico, A. Insolia, J. Phys. **G40** (2013) 015201; A.A. Arkhipov, arXiv:hep-ph/0607265; R. Ruffini, G.V. Vereshchagin, S.-S. Xue, arXiv:1503.07749.

[24] J.H. Ruan, Z.Q. Shen, J.F. Yang and W. Zhu, Nucl. Phys. **B760** (2007) 128.

[25] P. Abreu et al. [The Pierre Auger Collaboration],Phys. Rev. Lett. **109** (2012) 062002.

[26] X.R. Chen, J.H. Ruan, R. Wang, P.M. Zhang and W. Zhu, Int. J. Mod. Phys. **El23** (2014) 145005.

[27] V.S. Fadin and L,N. Lipatov, Phys. Lett. **B429** (1998) 127.

[28] D. Kharzeev and E. Levin, Phys. Lett. **B523** (2001) 79.

[29] S. Banerjee, J. A. Yorke, C. Grebogi, Phys. Rev. Lett. **80** (1998) 3049; A. Potapov, M. K. Ali, Phys. Lett. **A277** (2000) 310; A. Priel, I. Kanter, Europhys. Lett. **51** (2000) 230.

[30] W. Zhu, D. L. Xue, K. M. Chai and Z. X. Xu, Phys. Lett. **B317** (1993) 200.

[31] W. Zhu, Kangmin Chai and Bo He, Nucl. Phys. **B427** (1994) 525; W. Zhu, Kangmin Chai and Bo He, Nucl. Phys. **B449** (1995) 183; W. Zhu, Nucl. Phys., **B551** (1999) 245-274; W. Zhu and J.H. Ruan, Nucl. Phys., **B559** (1999) 378.

[32] W. Zhu, J.H. Ruan, J.F. Yang and Z.Q. Shen, Phys. Rev. **D68** (2003) 094015; W. Zhu, J.H. Ruan and F.Y. Hou, Int. J. Mod. Phys. **E22** (2013) 1350013.

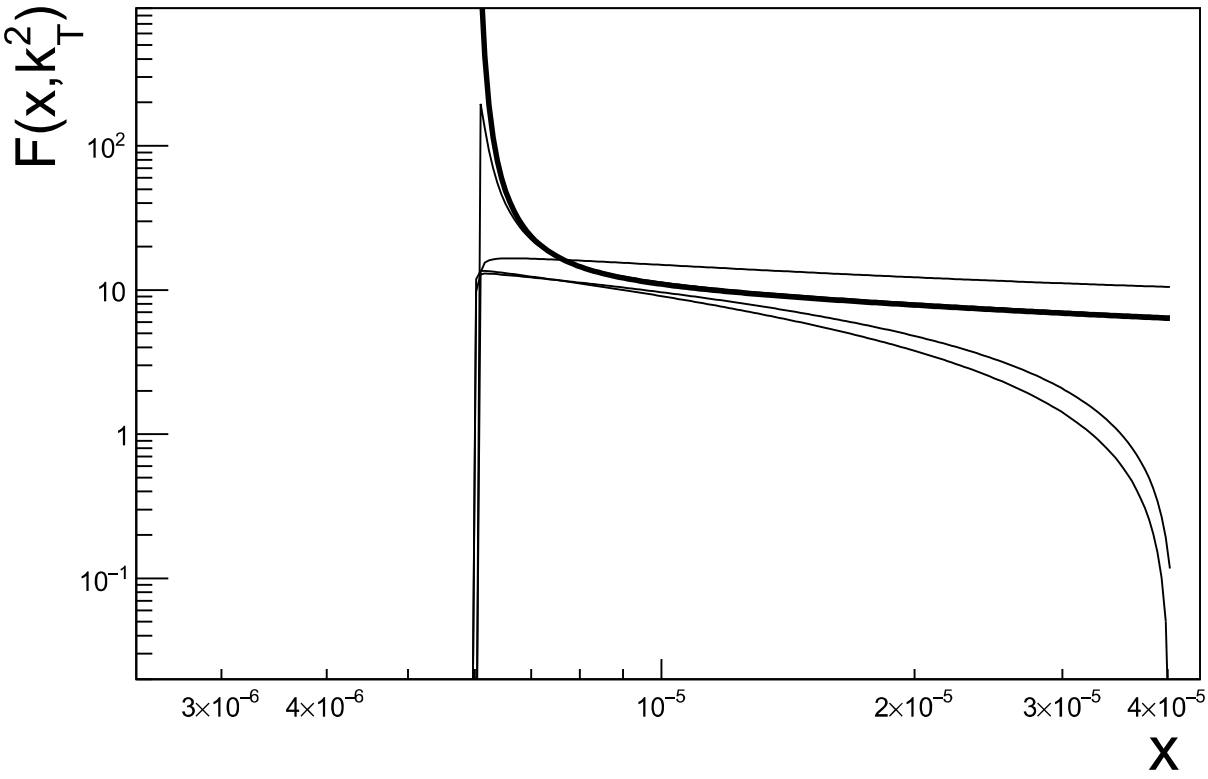

Figure 1: x-dependence of $F(x, k_T^2)$ using the GBW input with different momenta (from top on the right) $k_T^2 = 1, 0.668, 0.654, 10$ and 50 GeV^2, where the thick line ($k_T^2 = k_c^2 = 0.654\ GeV^2$) presents the antishadowing effect. This figure shows that the gluons at $x < x_c = 6 \times 10^{-6}$ converge to a state with $k_c^2 = 0.654\ GeV^2$ at $x_c = 6 \times 10^{-6}$.

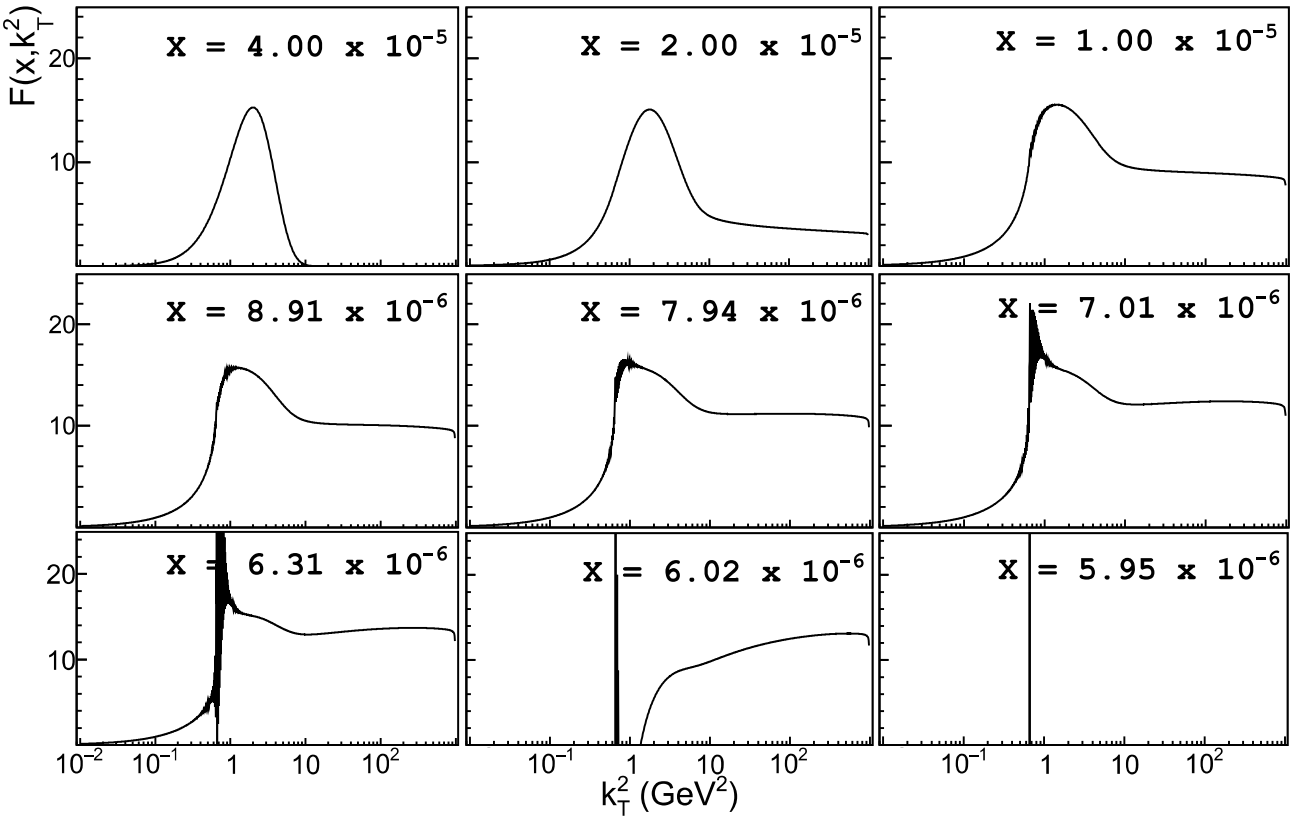

Figure 2: k_T^2-dependence of $F(x, k_T^2)$ using the GBW input at different values x, it shows clearly an evolution from the GBW saturated input at $x_0 = 4 \times 10^{-5}$ to a condensed state, which has a sharp peak in the distribution.

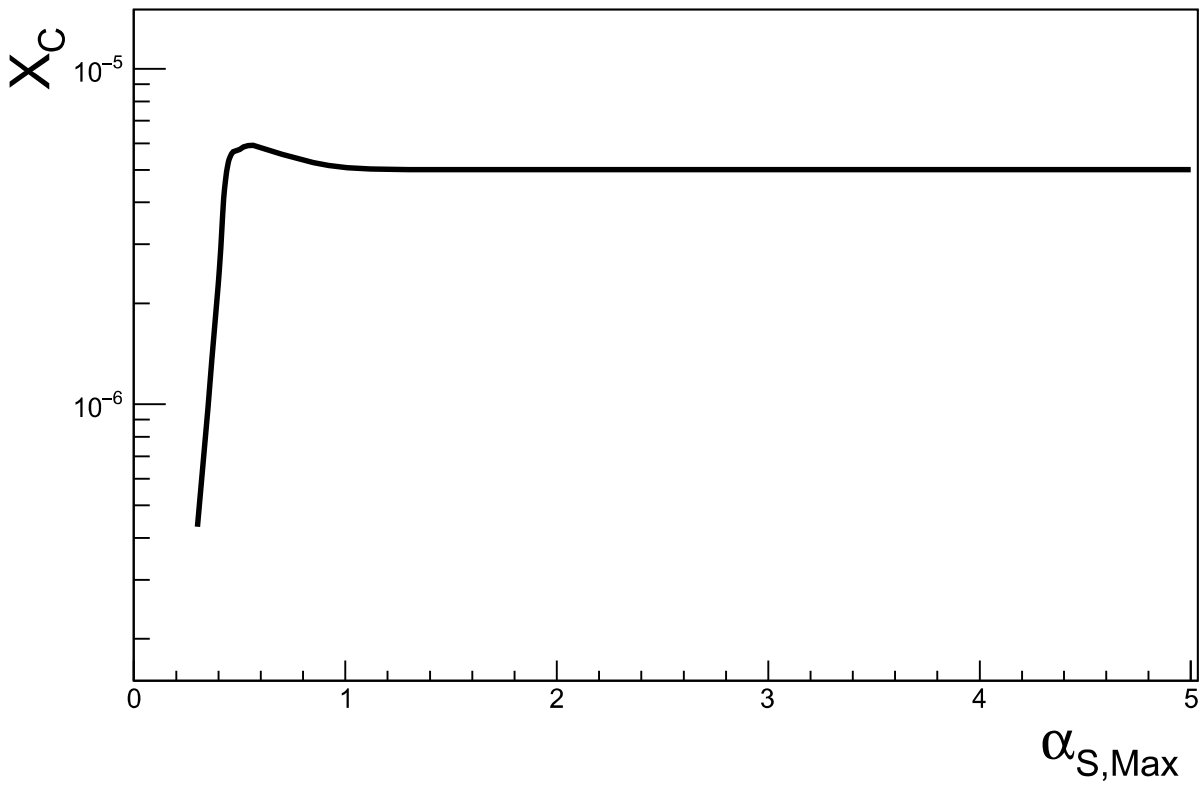

Figure 3: The value of x_c with different $\alpha_{s,Max}$ in Eq. (2.3).

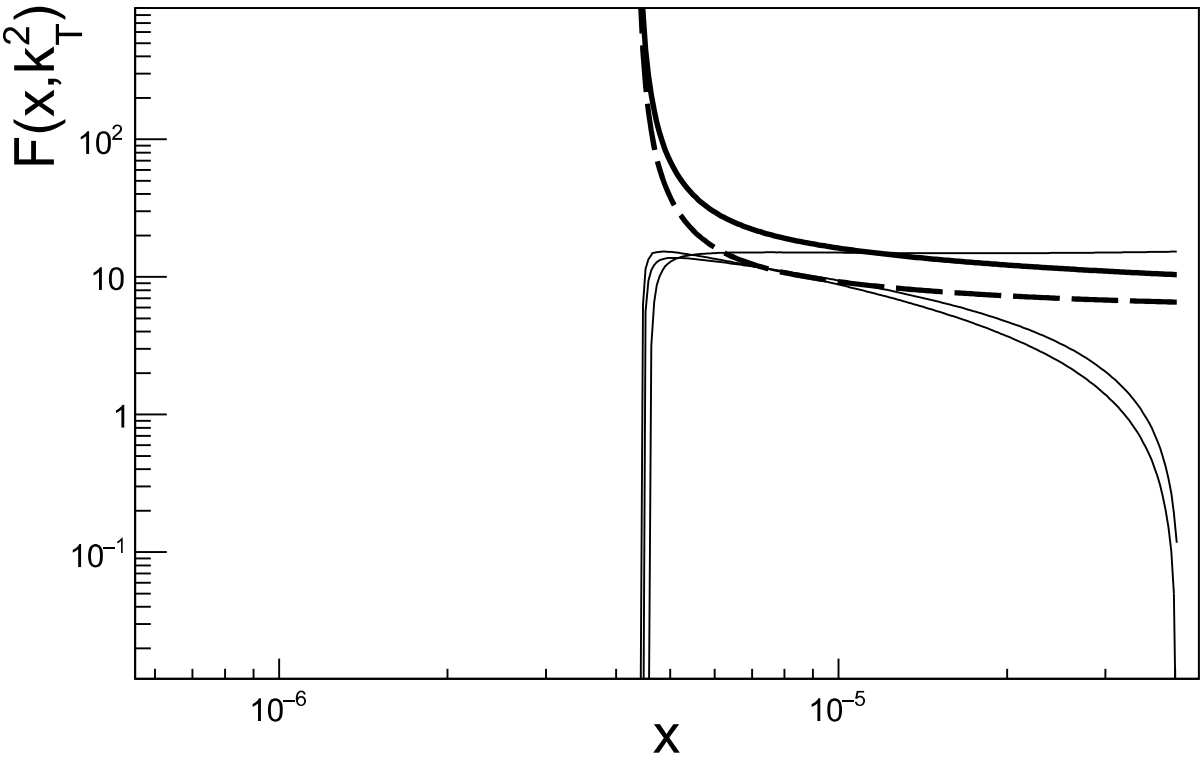

Figure 4: Similar to Fig. 1 but using Eq. (2.4) to replace Eq. (2.3): (from top on the right) $k_T^2 = 1, 0.668, 2, 10$ and $50\ GeV^2$. The dashed lines are added by using Eq. (2.4).

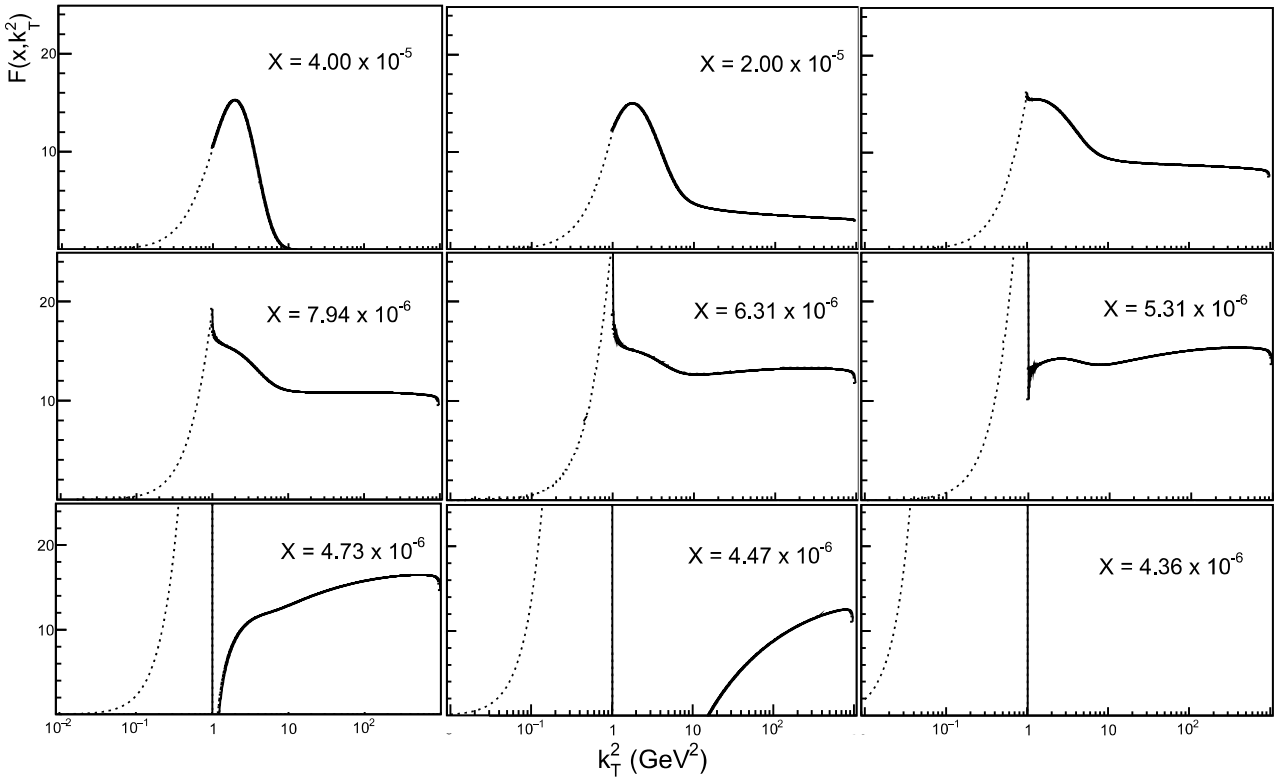

Figure 5: Similar to Fig. 2 but using Eq. (2.4) to replace Eq. (2.3). The dashed lines are added by using Eq. (2.4). One can find the dashed lines deform the condensation information.

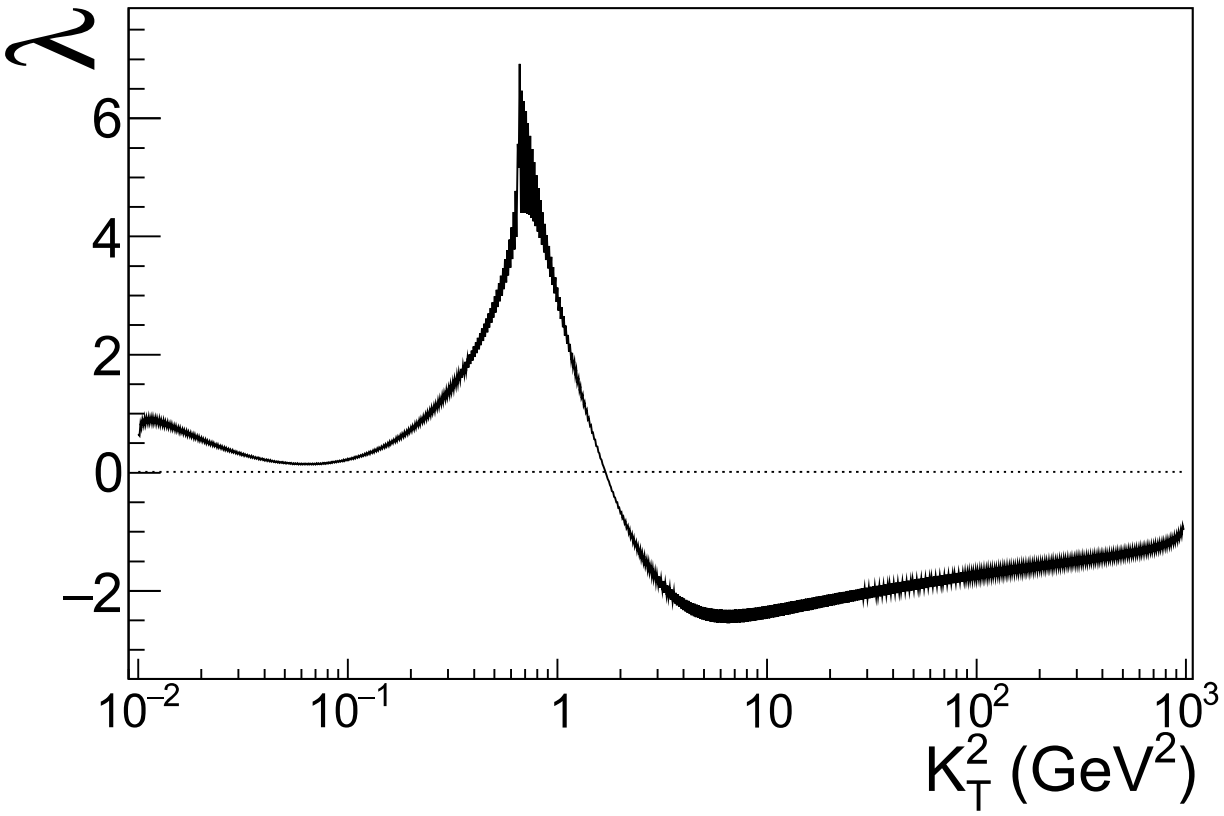

Figure 6: The Lyapunov exponents corresponding to Figs. 1 and 2. The larger positive domain, which is not mix with the negative exponents around k_c^2, implies that the solution is the robust chaos.

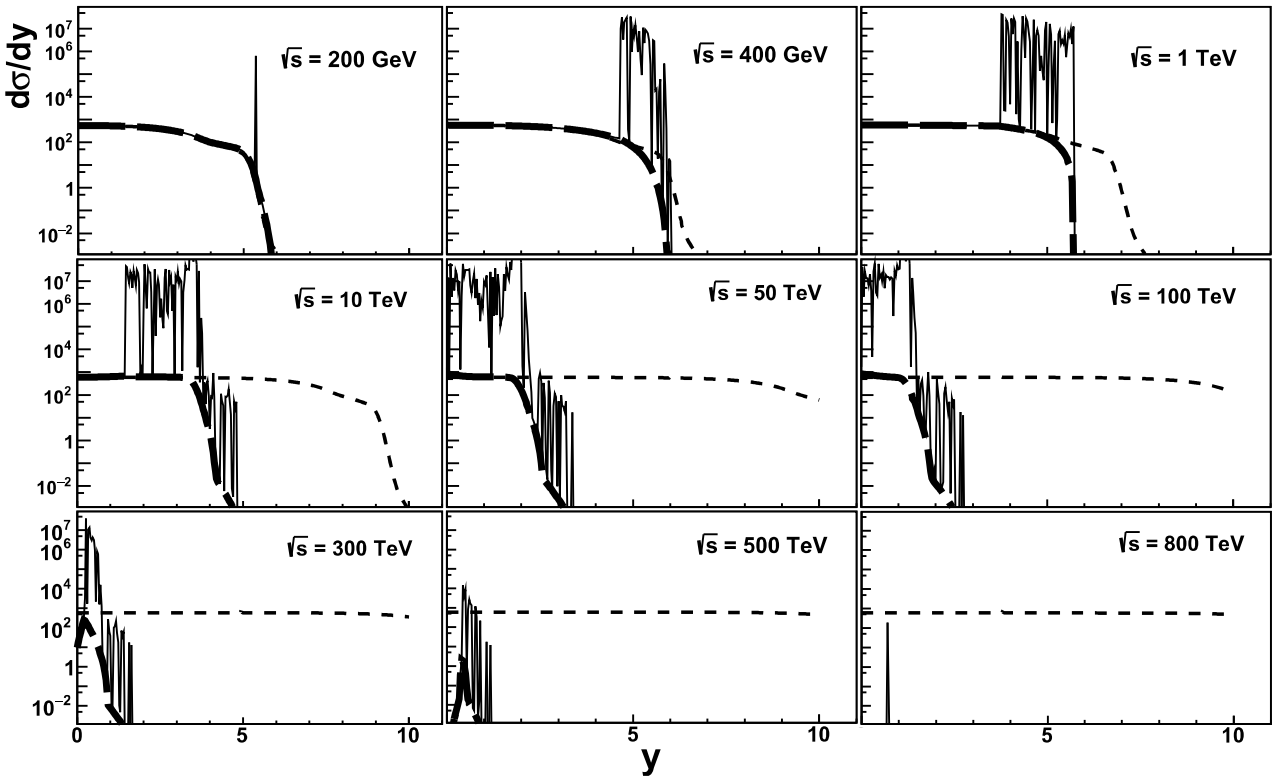

Figure 7: Inclusive gluon rapidity distribution in proton-proton collision using Eq. (3.2) and input (2.2) at different energy $\sqrt{s}$. The results show the large fluctuations are arisen by the gluon condensation. The broken lines are the results after removing the peak distribution from $F(x, \underline{k}^2)$; the dashed lines are the results using Eq. (2.2)$\times(1-x)^4$ without QCD evolution.

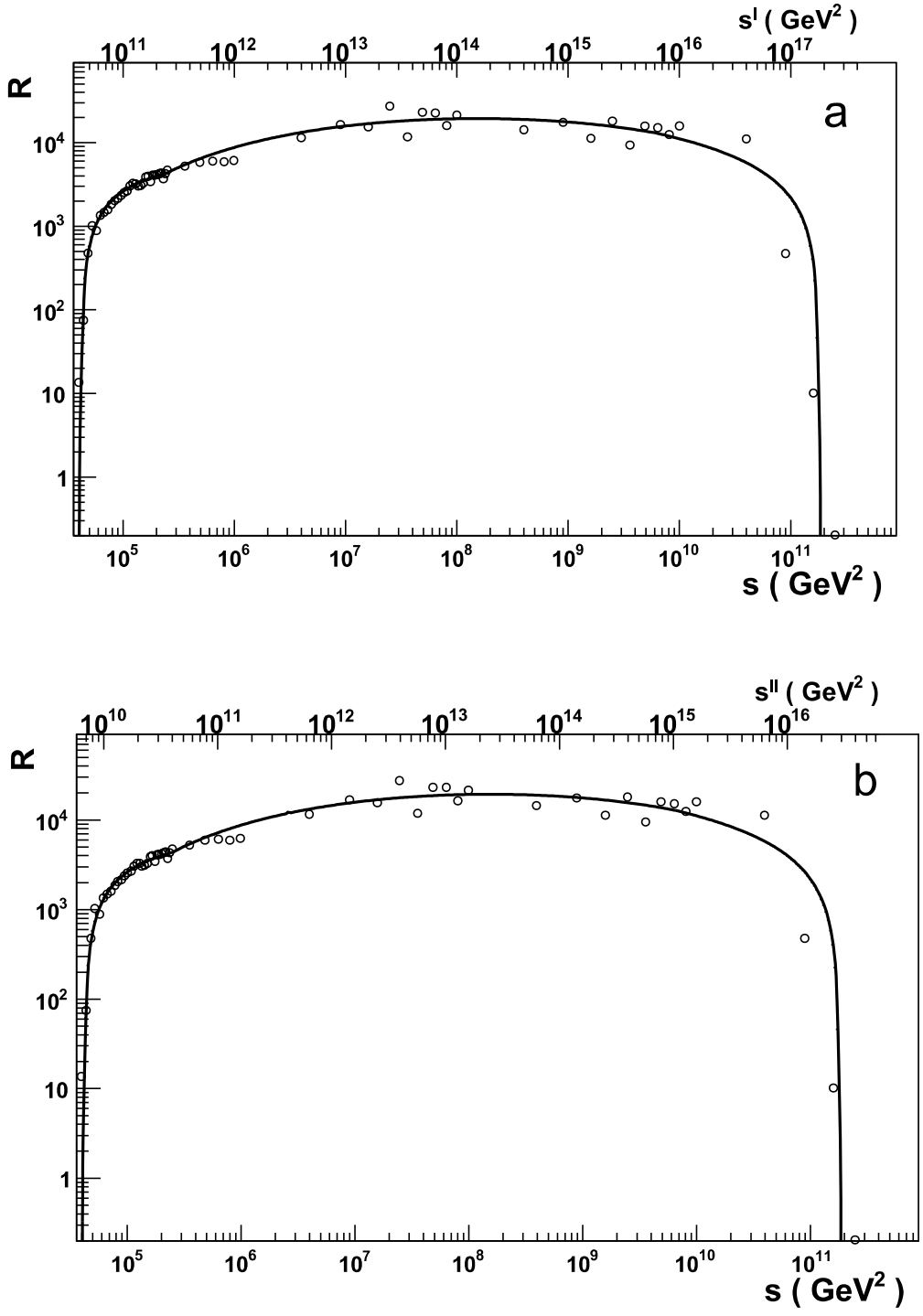

Figure 8: (a) Rate R(s) defined by Eq. (4.3) in the example $x_c = 6 \times 10^{-6}$. The top scale s^I corresponds to $x_c^I = 6 \times 10^{-12}$; (b) Similar to (a) but the top scale s^{II} corresponds to $x_c^{II} = 4 \times 10^{-11}$.

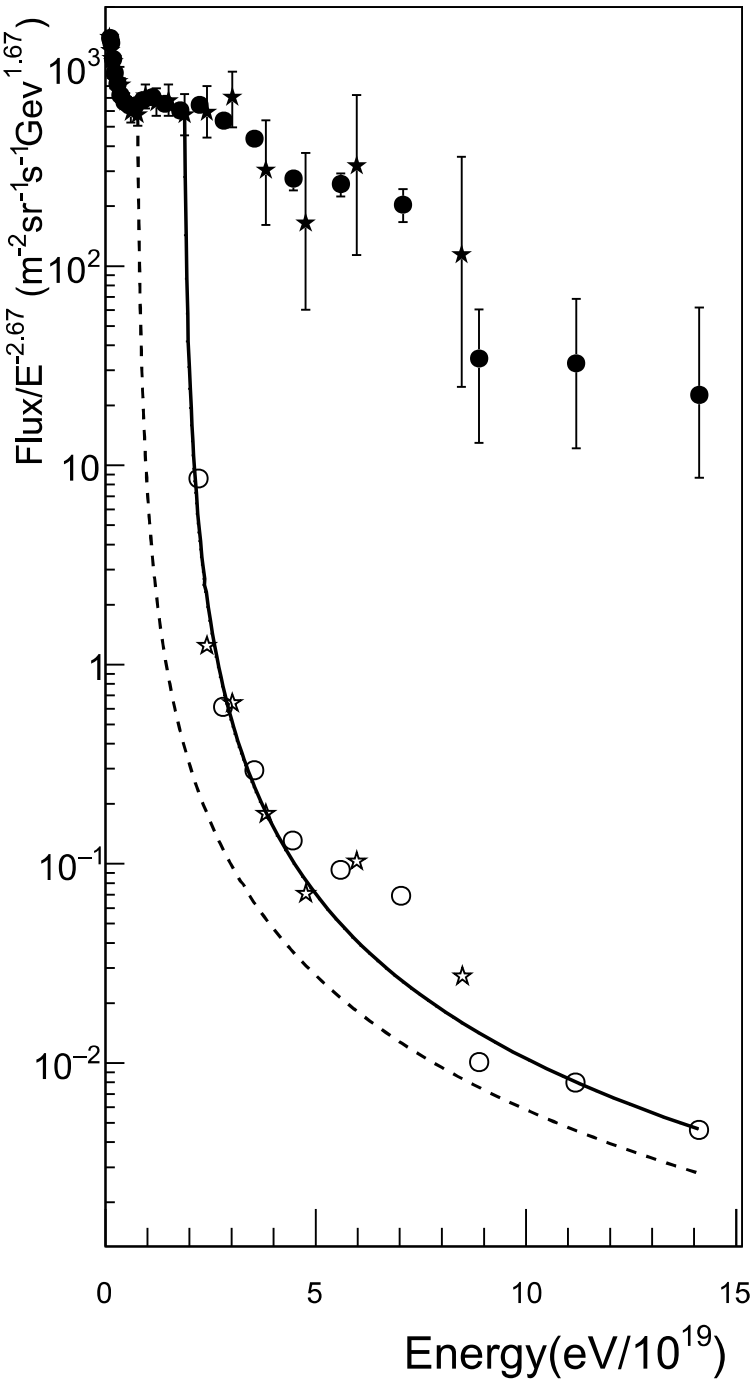

Figure 9: The UHECR spectrum measured by the Auger Collaborations [25] (solid points) and after deducting the contributions of the gluon condensation if $x_c^I = 6 \times 10^{-12}$ (open points) using Fig. 8(a); the solid line is a smoothing result; the dashed line is similar to the solid line but using $x_c^{II} = 4 \times 10^{-11}$ and Fig. 8(b). The spectrum has been multiplied by $E^{2.7}$.

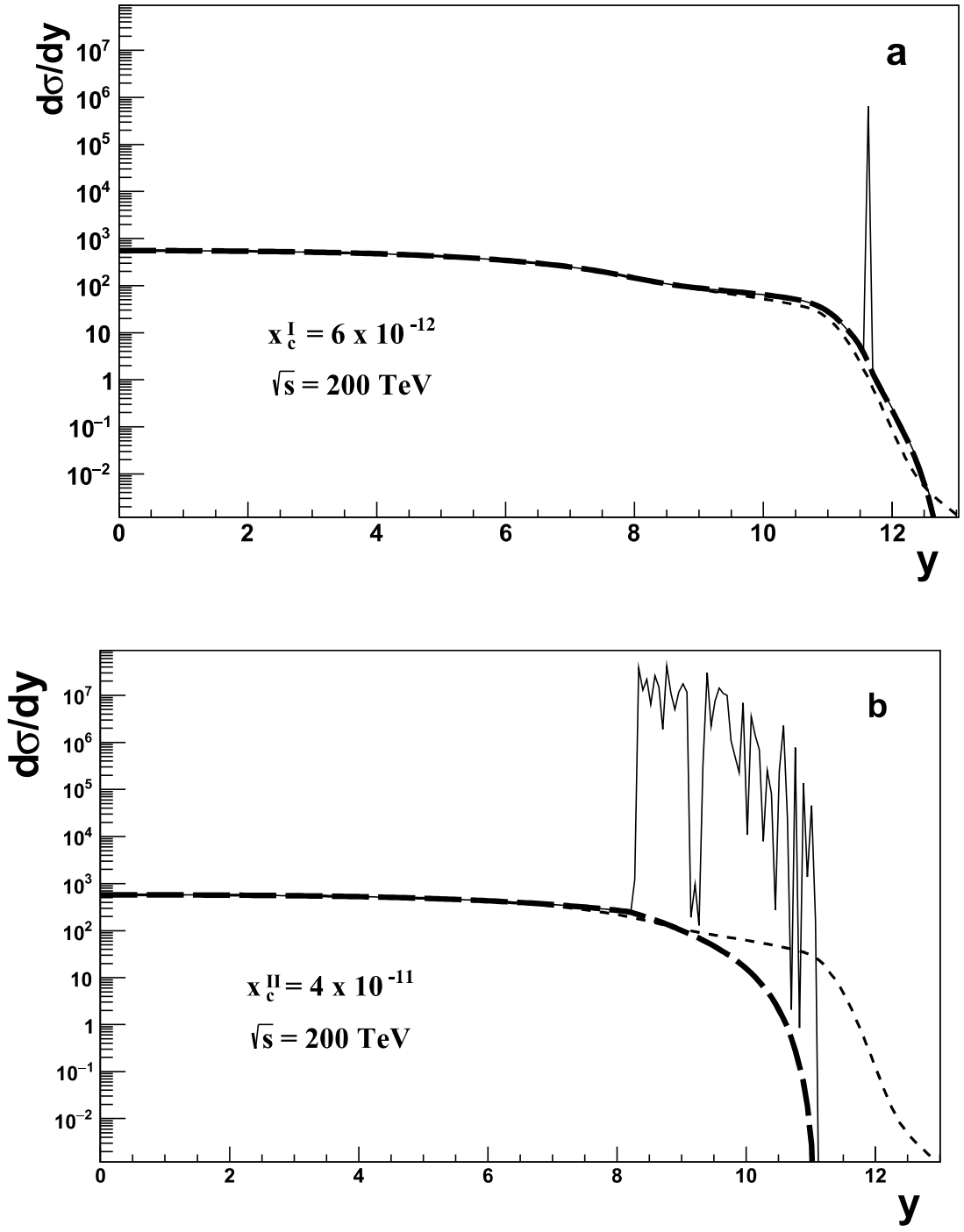

Figure 10: Predicted rapidity distributions of the gluon jets in proton-proton collision at $\sqrt{s} = 200\ TeV$ (a) $x_c^I = 6 \times 10^{-12}$; (b) $x_c^{II} = 4 \times 10^{-11}$. The broken lines are the results after removing the peak-like distribution from $F(x, k_T^2)$; the dashed lines are the results without QCD evolution. The longitudinal sale is un-normalized.

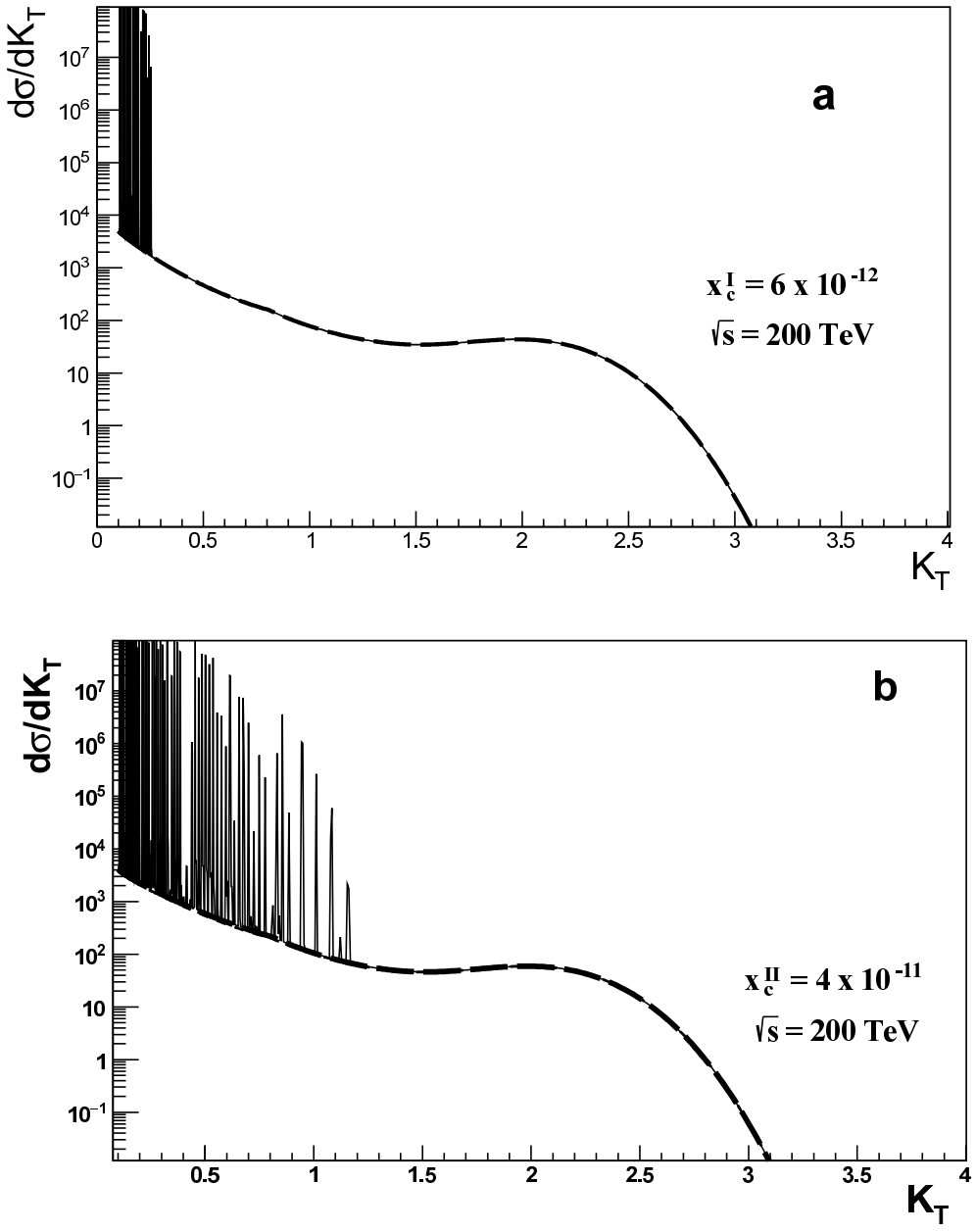

Figure 11: Predicted k_T-distributions of the gluon jet in proton-proton collision at $\sqrt{s} = 200\ TeV$, (a) $x_c^I = 6 \times 10^{-12}$; (b) $x_c^{II} = 4 \times 10^{-11}$. We call this structure as the gluon-jet bursts. The broken lines are the results after removing the peak-like distribution from $F(x, k_T^2)$; the dashed lines are the results without QCD evolution. The longitudinal sale is un-normalized.

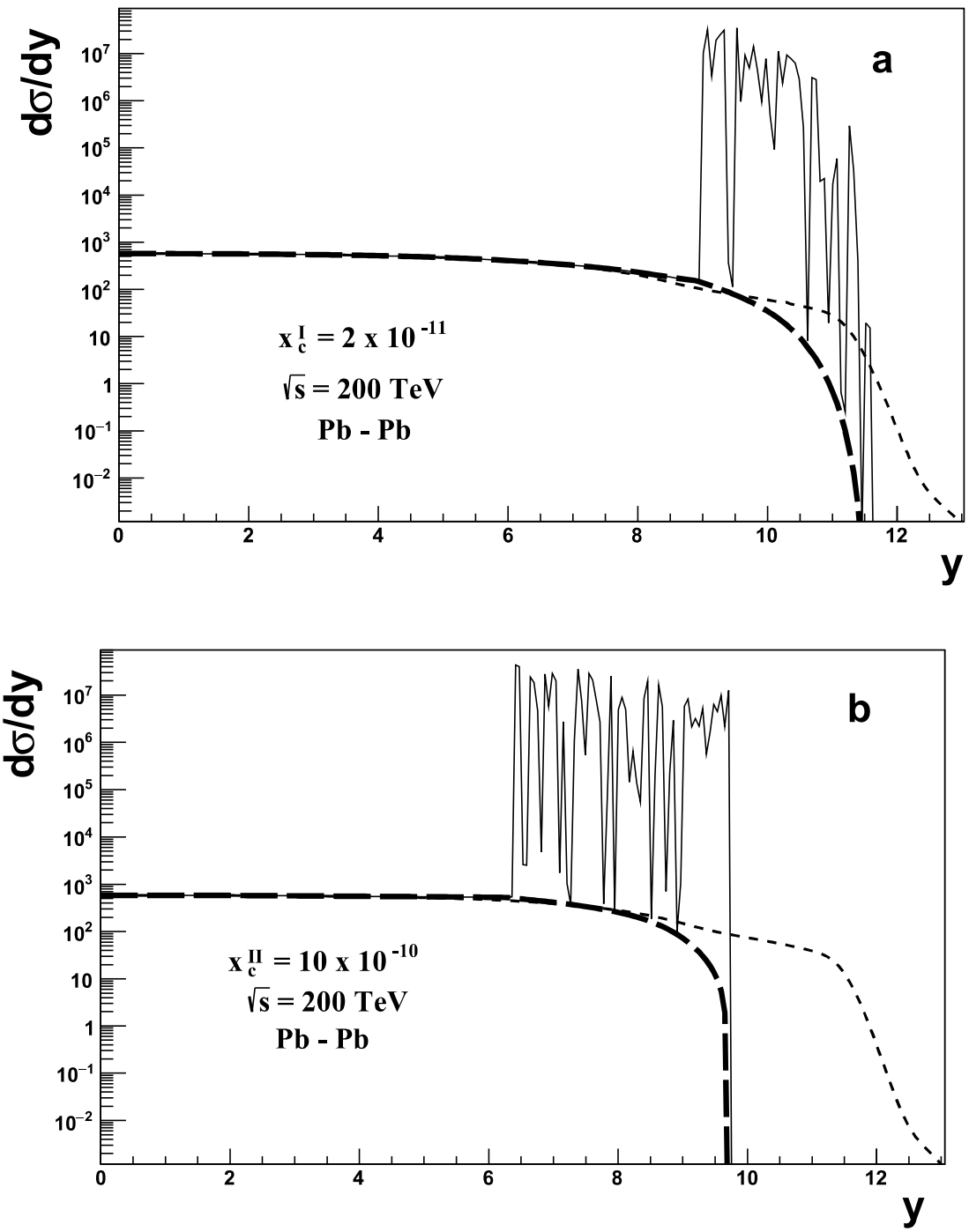

Figure 12: Predicted rapidity distributions of the gluon jets in Pb-Pb collision at $\sqrt{s} = 200\ TeV$ (a) $x^I_{c,Pb-Pb} = 2 \times 10^{-11}$; (b) $x^{II}_{c,Pb-Pb} = 10^{-10}$. The broken lines are the results after removing the peak-like distribution from $F(x, k_T^2)$; the dashed lines are the results without QCD evolution. The longitudinal sale is un-normalized.

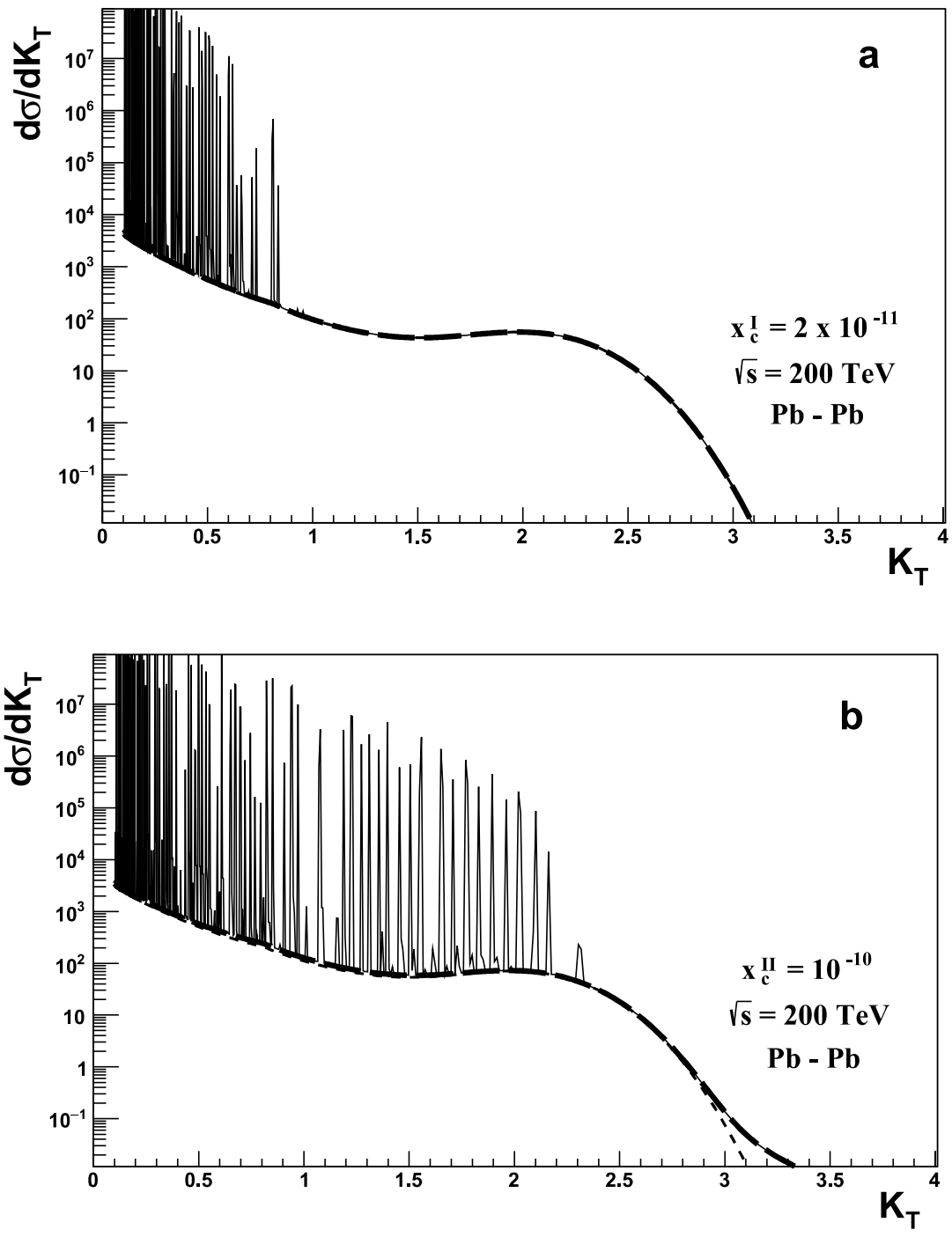

Figure 13: Predicted k_T-distributions of the gluon jet in Pb-Pb collision at $\sqrt{s} = 200\,TeV$, (a) $x^I_{c,Pb-Pb} = 2 \times 10^{-11}$; (b) $x^{II}_{c,Pb-Pb} = 10^{-10}$. The broken lines are the results after removing the peak-like distribution from $F(x, k_T^2)$; the dashed lines are the results without QCD evolution. The longitudinal sale is un-normalized.

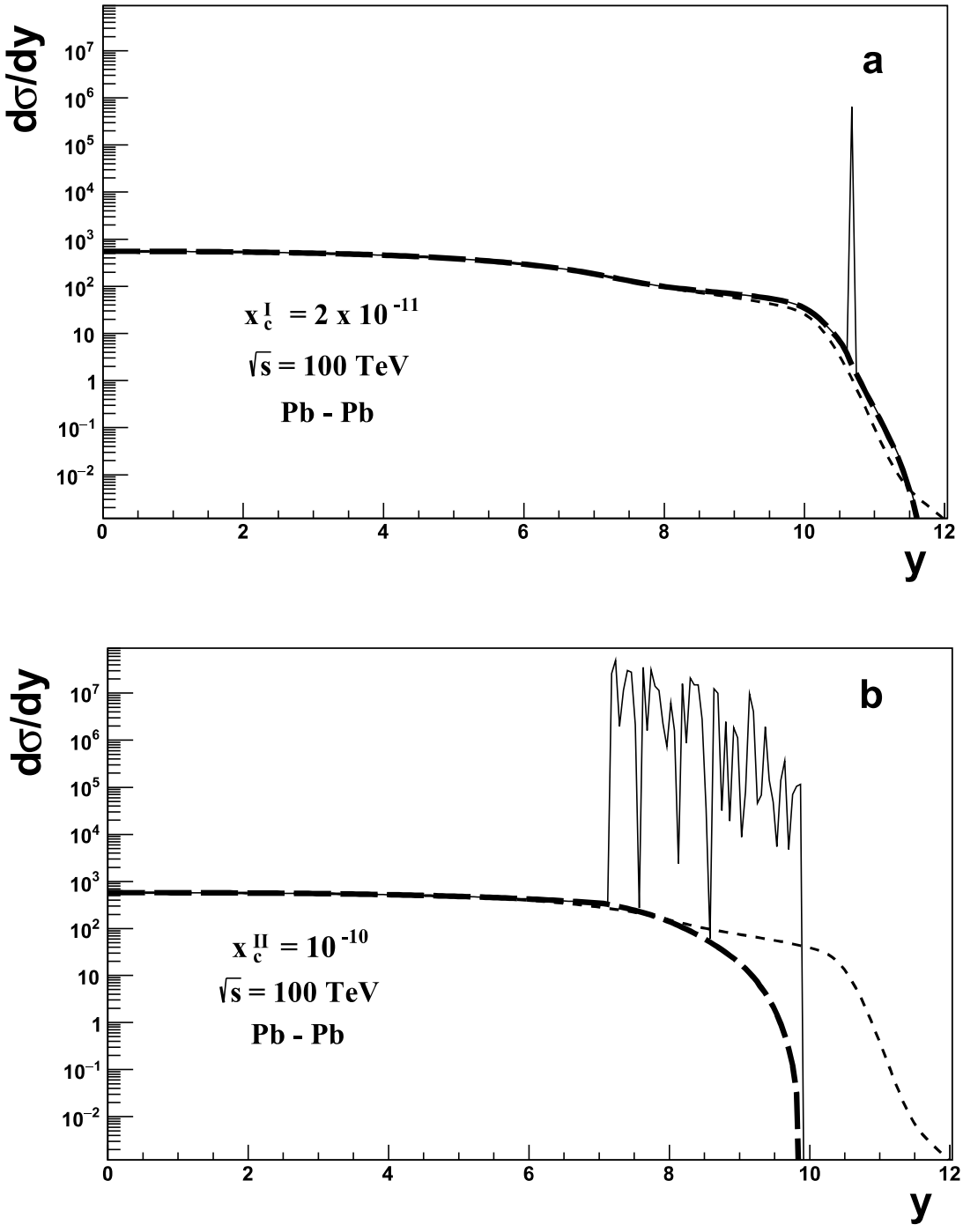

Figure 14: Similar to Fig. 12 but for the rapidity distributions of the gluon jets in Pb-Pb collision at $\sqrt{s} = 100\ TeV$ (a) $x^I_{c,Pb-Pb} = 2 \times 10^{-11}$; (b) $x^{II}_{c,Pb-Pb} = 10^{-10}$.

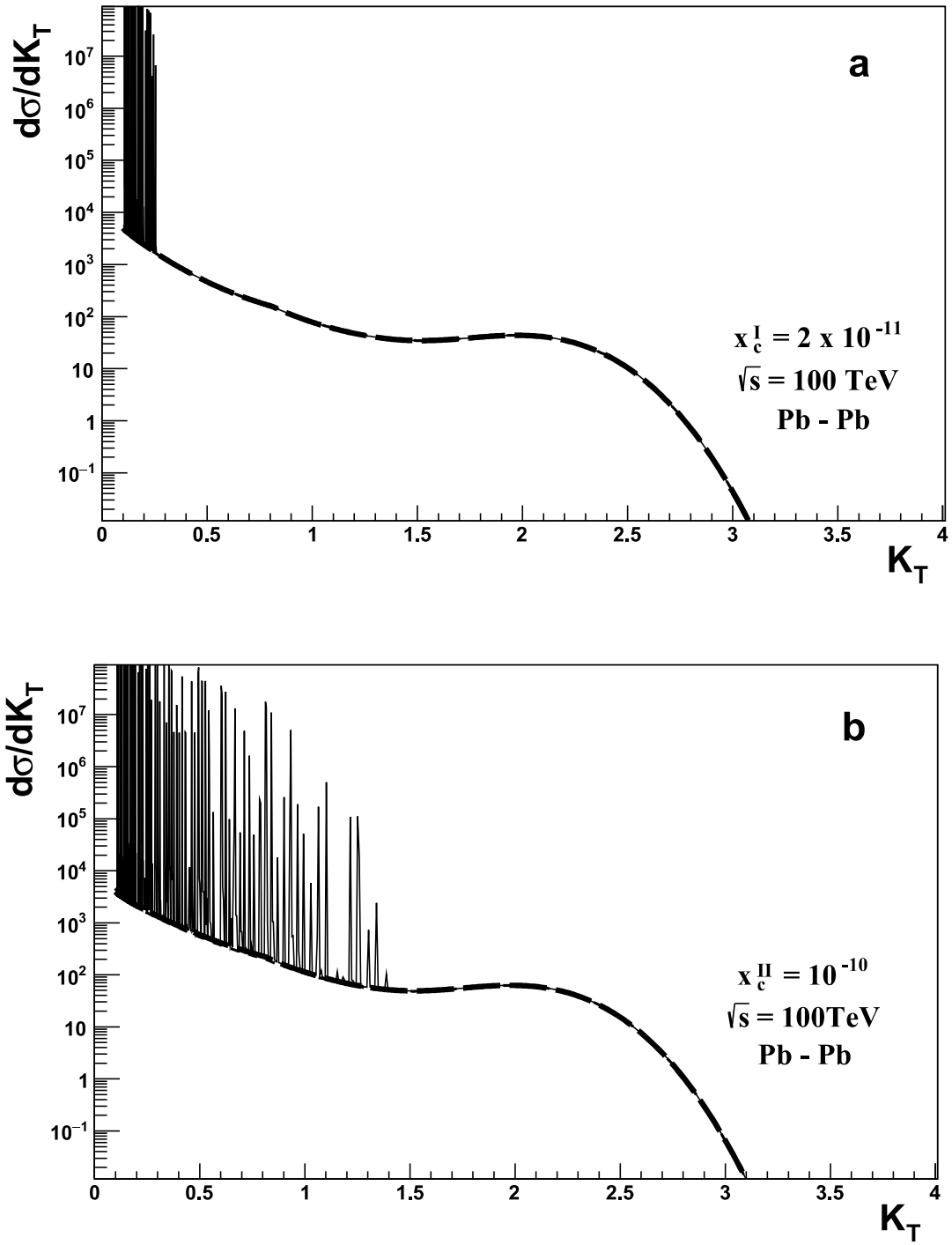

Figure 15: Similar to Fig. 13 but for the k_T-distributions of the gluon jet in Pb-Pb collision at $\sqrt{s} = 100\ TeV$, (a) $x^I_{c,Pb-Pb} = 2 \times 10^{-11}$; (b) $x^{II}_{c,Pb-Pb} = 10^{-10}$.

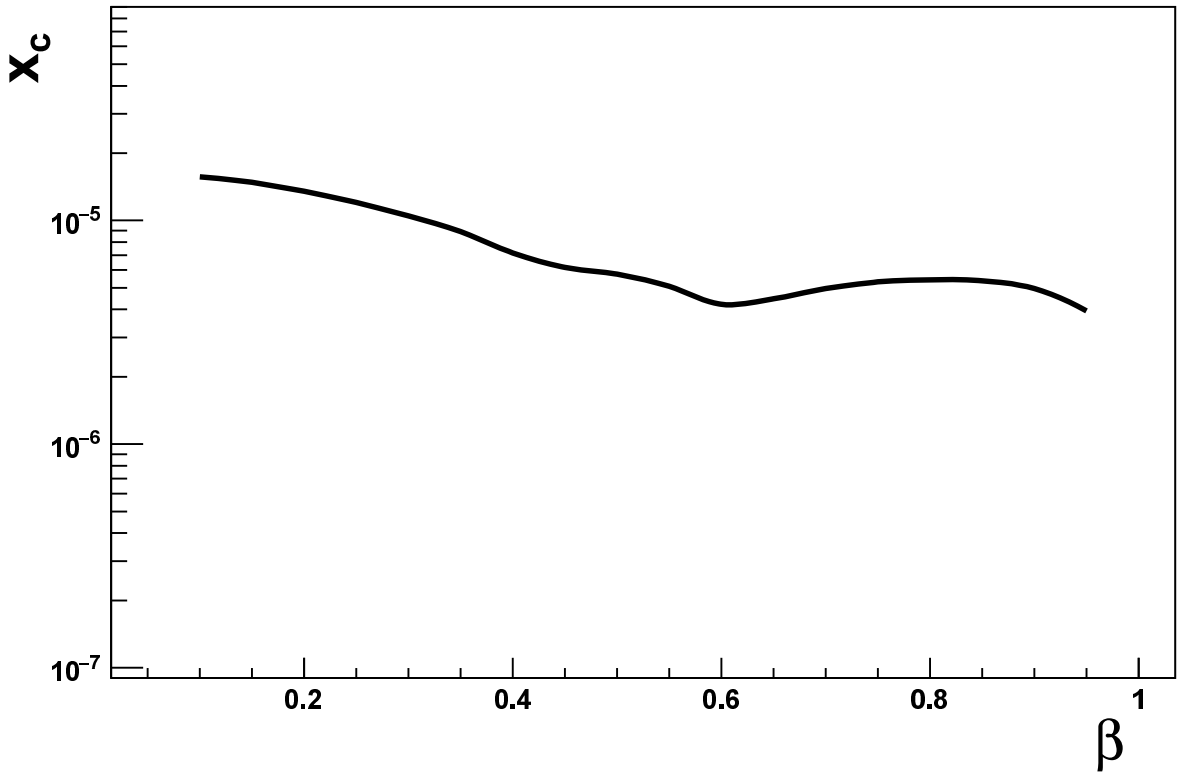

Figure 16: The critic value x_c with different β in Eq. (6.2). The result shows that the chaotic solution is insensitive to the parameter β in its reasonable range.

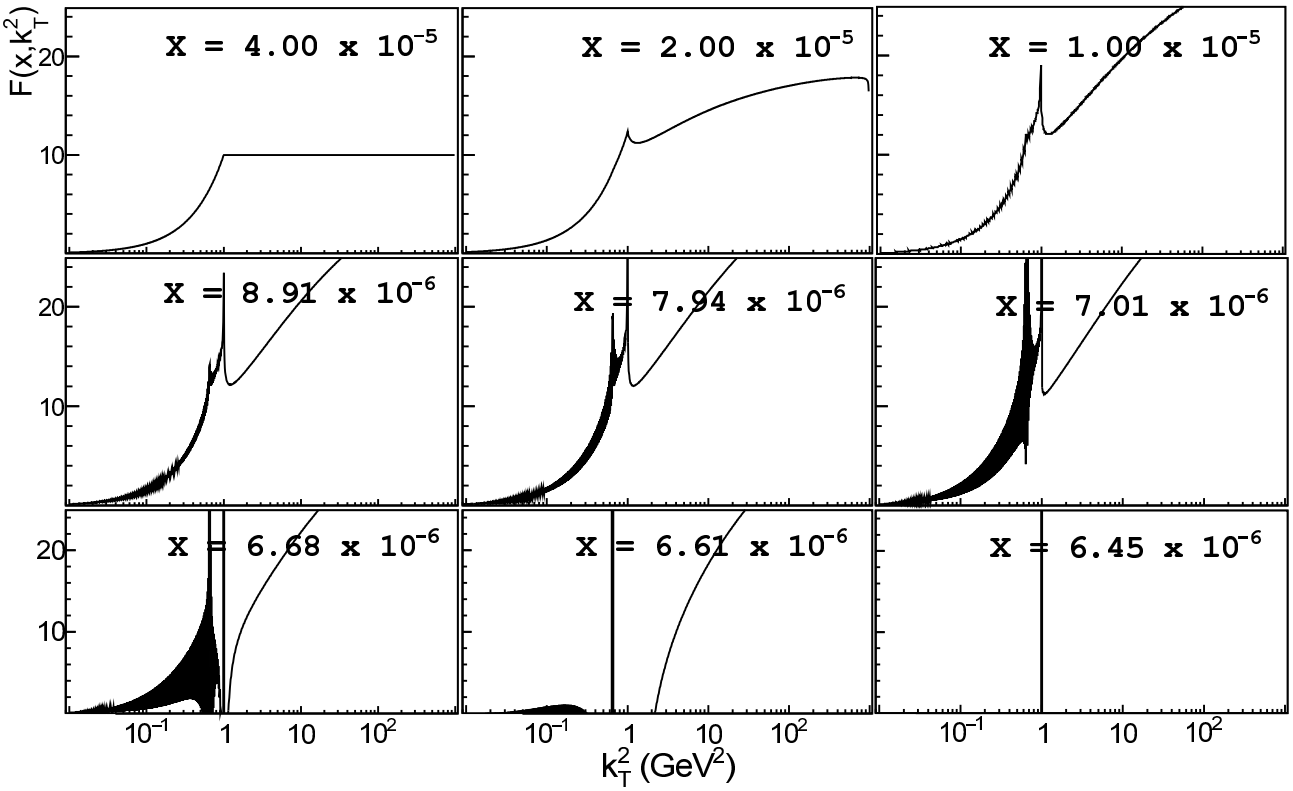

Figure 17: Similar to Fig. 2 but using the KL input Eq. (6.3). The results show that two maximum peaks corporate to one peak at $x \to x_c$.

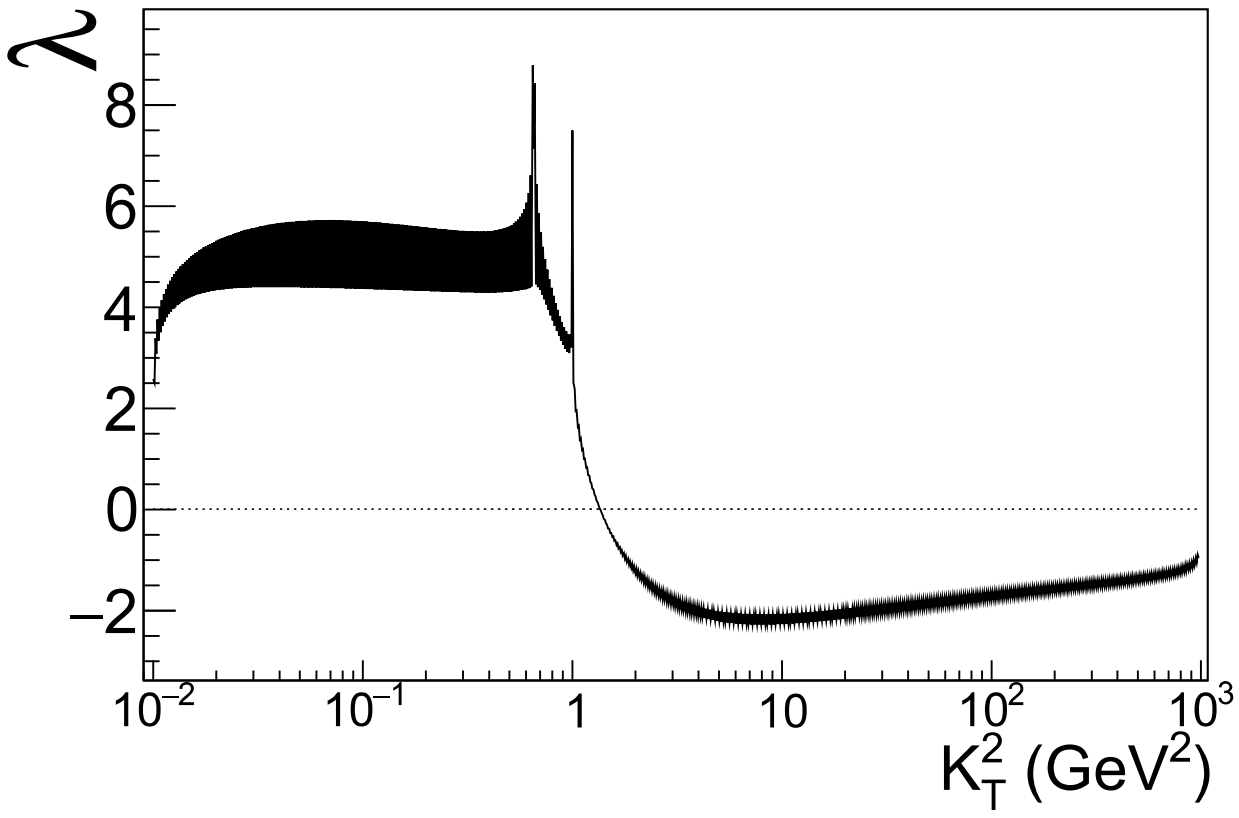

Figure 18: The Lyapunov exponents corresponding to Fig. 17.

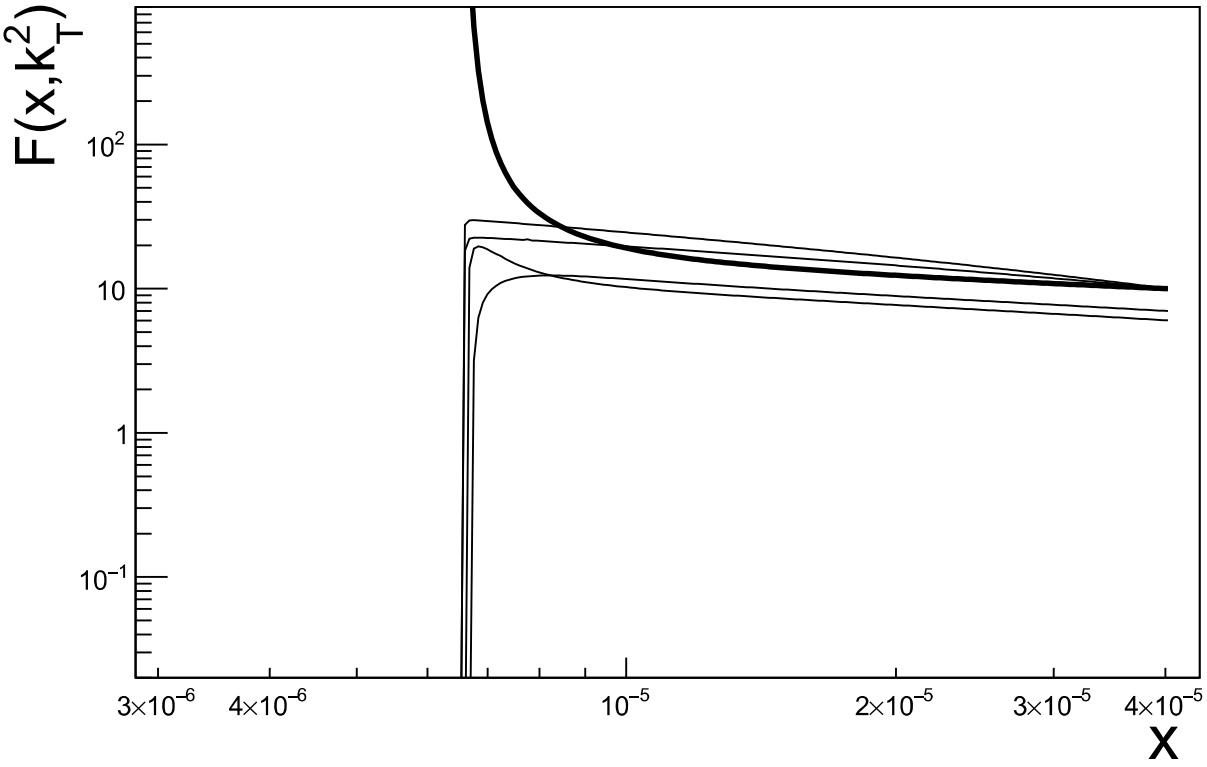

Figure 19: Similar to Fig. 1 but using the KL input Eq. (6.3). The lines from top on the right are $k_T^2 = 50, 10, 1, 0.7$ and $0.6\ GeV^2$, where the thick line ($k_T^2 = k_c^2 = 1\ GeV^2$) presents the antishadowing effect. The results show that the gluons at $x < x_c = 6.45\times10^{-6}$ converge to a state with $k_c^2 = 1\ GeV^2$ at $x_c = 6.45 \times 10^{-6}$.